Modeling and Control of A Two-bus System With Grid-forming and Grid-following Converters

Zou, Zhixiang; Tang, Jian; Wang, Xiongfei; Wang, Zheng; Chen, Wu; Buticchi, Giampaolo; Liserre, Marco

Published in:
IEEE Journal of Emerging and Selected Topics in Power Electronics

DOI (link to publication from Publisher):
10.1109/JESTPE.2022.3182366

Publication date:
2022

Document Version
Accepted author manuscript, peer reviewed version

Modeling and Control of A Two-bus System With Grid-forming and Grid-following Converters

Zhixiang Zou, *Senior Member, IEEE,* Jian Tang, *Student Member, IEEE,* Xiongfei Wang, *Senior Member, IEEE,* Zheng Wang, *Senior Member, IEEE,* Wu Chen, *Senior Member, IEEE,* Giampaolo Buticchi, *Senior Member, IEEE,* and Marco Liserre, *Fellow, IEEE*

***Abstract*—The utilization of power converters in a distribution network could give rise to stability problems, especially when the penetration is high. The existing literature studies the modeling and stability of converters with specific control or synchronization methods. However, the types or the control schemes of converters are normally different in an actual grid, and moreover the line impedance plays an important role on the network stability. In this regard, this paper aims at studying the modeling and stability issues of a two-bus electric network with both grid-forming and grid-following converters. The main purpose is to provide design guidelines and solution of two-bus system with converters for stable operation. The interactions between the converters in various scenarios will be investigated by considering the effect of line impedance. More importantly, a filter-based stabilized control strategy will be proposed for the grid-forming converters to mitigate the oscillation in the network. Simulation and experimental results are provided to validate the effectiveness of the theoretical analysis and control strategy.**

***Index Terms*—Grid-forming converter, grid-following converter, small-signal model, stability analysis, filter-based control.**

I. Introduction

A Fundamental change of paradigm has been proposed in the context of power systems, namely the increasing utilization of power converters. The stability of an electric grid dominated by the power converters has drawn wide attentions, particularly focusing on the topics including system modeling [1], stability assessment [2]–[4], and stabilized control [5]–[7].

In the literature, researchers focused on the modeling and stability assessment of single power converter or parallel ones with identical converter type [8]–[12]. The detailed small-signal models of grid-following (GFL) converter (e.g., synchronized by phase-lock loops) have been developed by using the impedance modeling method in [8]–[10]. The models can be easily extended to the paralleled system for the stability assessment [12], [13] and even for the transient study under certain circumstance [14]. Similarly, for another major category of converters, modeling and stability analysis of grid-forming (GFM) converters (e,g, utilize droop control, virtual synchronous machine, etc.) have been investigated in [15]–[18]. In addition, the stability of a network consists of hybrid types of converters has been studied in [19], [20]. In particular, a generic stability criterion based on bus node impedance has been proposed in [21] for hybrid types of converters. However, there are some fundamental issues considering the modeling and stability analysis: 1) The simplified models have mostly been used in the stability analysis of the overall network, for instance, the synchronization as well as some of the control loops and network parameters are neglected. 2) Most of the published literature has focused on the stability assessment for certain system configuration, whereas the interaction mechanism of hybrid types of converters has not been comprehensive studied. 3) The key parameters of a network with hybrid types of converters has been seldom investigated, the design guidelines and the optimal ranges of the parameters with the stability concern are required.

Besides, existing works had proposed stabilized control strategies for power converters to mitigate harmonic instability. The most classical solution is to use active damping to particularly address resonance issues [22], [23]. Further works [5] and [6] employ converter-based multifunctional devices to increase the damping factor of the system or decouple the electromagnetic interactions among different converters. These methods are more effective to deal with harmonic instability, but they are sensitive to parameter uncertainties and instability types [24]. Moreover, most of the proposed methods are designed to mitigate stability issues caused by GFL converters. For the GFM converters, stabilized control strategy is still missing.

To address the above-mentioned issues, this paper investigates the stability of a two-bus system with both GFL and GFM converters in different scenarios. Design guidelines of various parameters and a filter-based stabilized control for GFM converter are proposed to ensure stable operation of the system. The main contributions include:

1) The impedance-based models for both GFL and GFM converters have been developed in consideration of the core elements involved, using a general small-signal modeling procedure.

2) The stability issues of a two-bus system with hybrid types of converters in different scenarios have been comprehensively studied.

Z. Zou, J. Tang, Z. Wang, W. Chen are with the School of Electrical Engineering, Southeast University, 210096 Nanjing, China (e-mail: zzou@seu.edu.cn).

X. Wang is with the Department of Energy Technology, Aalborg University, 9220 Aalborg, Denmark.

G. Buticchi is with University of Nottingham Ningbo China, 315100 Ningbo, China.

M. Liserre is with the Chair of Power Electronics, Kiel University, 24143 Kiel, Germany.

This work was supported in part by the National Natural Science Foundation of China under Grant 52007033 and in part by Jiangsu Provincial Key Laboratory of Smart Grid Technology and Equipment, Southeast University.

Manuscript received April 19, 2021; revised August 16, 2021.

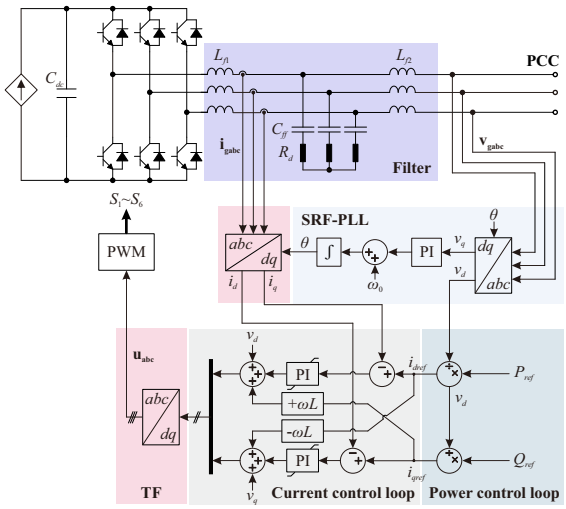

Fig. 1. Typical system configuration of a grid-following converter.

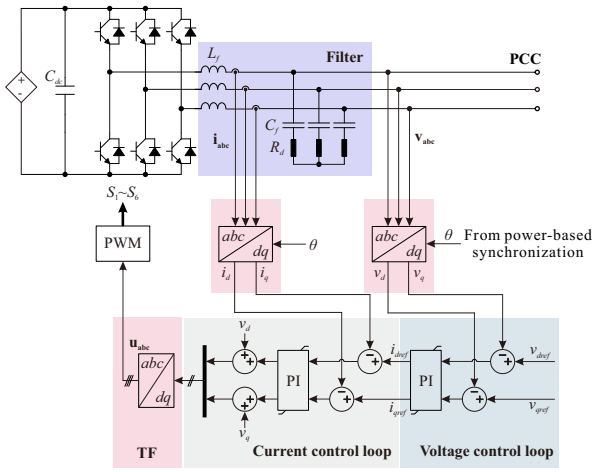

Fig. 2. Typical system configuration of a grid-forming converter.

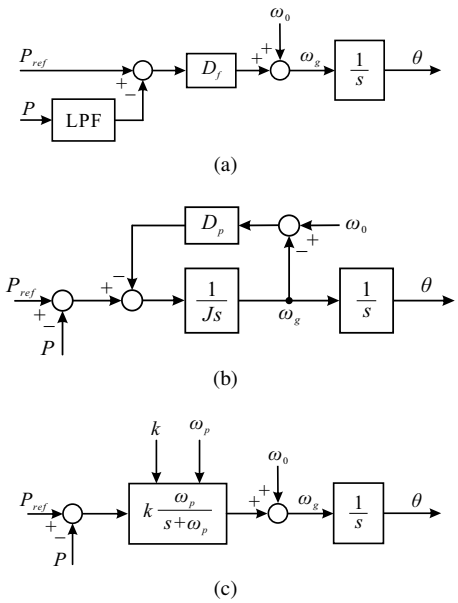

Fig. 3. Power-based synchronization methods for grid-forming converters: (a) frequency droop control, (b) virtual sysnchronous machine, and (c) synchronous power control.

3) Key parameters that determine the system stability have been identified, and design guidelines of the key parameters in different scenarios have been presented based on their stability regions.

4) A filter-based stabilized control strategy has been proposed and implemented in the GFM converter to mitigate oscillations of two-bus systems.

The paper structure is organized as follows. The system configurations of GFL and GFM converters with different synchronization methods are presented in Section II. The small-signal models of the typical GFL and GFM converters are then developed in Section III using a generalized procedure. Based on the models, the stability of a two-bus system with different converters is assessed in Section IV, the interactions between different converters are also studied in this section. The key parameters are identified in Section V using sensitivity analysis, the stability regions as well as the design guidelines of these parameters are presented in this section as well. The filter-based stabilized control strategy for GFM converter is proposed in Section VI. Simulation results and experimental tests are provided in Section VII to validate the effectiveness of the analysis and the proposed control. Conclusions are drawn in Section VIII.

II. Grid-following And Grid-forming Converters

Based on the control and operation, power converters in ac distribution grids can be classified into GFL and GFM converters. GFL converters are power-controlled or current-controlled, a GFL converter can be considered as a controlled current source with an equivalent admittance in parallel. During normal operation, it operates at unity power factor, while it can support the voltage profile by injecting reactive power upon the requests from the distribution system operator (DSO). GFL converters do not inherently preserve their phase shift as well as phase sequencing during grid-connected operation. As a result, a grid synchronization algorithm has to be used [25]. Fig. 1 shows the schematic and control block diagram of a standard GFL converter.

GFM converters regulate voltage and frequency, a GFM converter can be regarded as a controlled voltage source with an output impedance in series. Depending on different applications, the set-points can be either manually set (e.g., low-voltage converter of smart transformer [26]) or obtained from a power control loop (e.g., virtual synchronous machine (VSM), synchronverter [27], [28]). In particular, the power control loop not only determines the power injection into the grid, but also offers a synchronization mechanism that mimics the characteristics of synchronous generators. The multiloop voltage control strategy is usually employed by the GFM converter, due to its ease of implementation and excellent control performance in terms of power quality and dynamics [29]. Fig. 2 shows the schematic and control block diagram of a standard GFM converter.

Various power-based synchronization methods can be employed for the GFM converter to synchronize with the grid

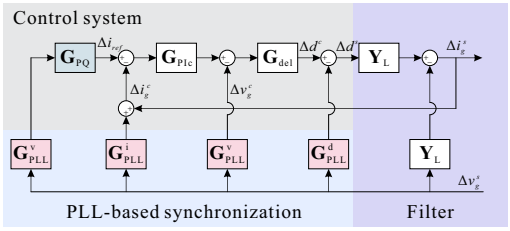

Fig. 4. Small-signal model of a GFL converter considering the synchronization effect.

[30]. In Fig. 3, three most common methods are presented including droop control [31], VSM-based control [27], and synchronous power control (SPC) [32]. Though these methods have been developed in different contexts, they present similarity in terms of transfer functions. According to the open-loop transfer functions, the three transfer functions are equivalent under certain conditions, which are [33]

$$D_p = \frac{1}{D_f} = \frac{1}{k}; \frac{1}{J} = D_f \omega_c = k\omega_p \tag{1}$$

If (1) is fulfilled, the GFM converters using different power-based synchronization will represent similar behaviors in terms of steady-state performance and static stability. Since the main purpose of this paper is to investigate the static stability, for the sake of simplicity, one of the synchronization methods (i.e., VSM-based control) will be selected in the modeling and analysis of GFM converters.

III. Generalized Model of Power Converters

In this section, a general modeling procedure considering the synchronization effect is proposed to develop models of GFL and GFM converters, which includes three steps:

Firstly, the small-signal models of the control system and the filter can be developed, respectively.

Secondly, the effect of synchronization will be considered, namely all the variables of the frame of the actual system will be converted to the variables coordinated by the synchronization.

Eventually, by combining the models of the previous two steps, the small-signal impedance model of the converter in the complex domain can be obtained.

A. Grid-following Converters

The small-signal model of a GFL converter is shown in Fig. 4. The multiloop control with the power outer loop and the current inner loop in the dq frame is developed in gray, while the filter is shown in purple. The effect of synchronization, namely the PLL, is highlighted by blue, while the pink blocks represent the Park transform and its inverse.

According to Fig. 4, the control system can be described by

$$\Delta \mathbf{d^c} = -\mathbf{G_{del}}(\Delta \mathbf{v_g^c} + \mathbf{G_{PIc}} \Delta \mathbf{i_g^c}) \tag{2}$$

and the filter can be represented by

$$\Delta \mathbf{i_g^s} = \mathbf{Y_L}(\Delta \mathbf{d^c} - \Delta \mathbf{v_g^s}) \tag{3}$$

TABLE I
System Parameters

Symbol	Quantity	Value
V_n	Nominal phase-to-neutral voltage (rms)	220 V
V_{dc}	dc-link voltage of converter	650 V
L_f	filter inductance of converter	3 mH
C_f	filter capacitance of converter	1.5 μF
f_s	sampling frequency	10 kHz
k_{ppll}	proportional gain of PLL	4.43
k_{ipll}	integral gain of PLL	3061
k_{pc}	proportional gain of GFL current loop	16
k_{ic}	integral gain of GFL current loop	600
J	virtual inertia	2
D_p	damping factor	63
K_q	Q-droop coefficient	0.0002
k_{pv}	proportional gain of GFM voltage loop	2
k_{iv}	integral gain of GFM voltage loop	500
k_{pi}	proportional gain of GFM current loop	5
k_{ii}	integral gain of GFM current loop	250

where $\Delta \mathbf{v_g^c}$ and $\Delta \mathbf{v_g^s}$ are the grid voltage perturbations in synchronized-frame and system frame, $\Delta \mathbf{i_g^c}$ and $\Delta \mathbf{i_g^s}$ are the converter current perturbations in synchronized-frame and system frame, $\mathbf{G_{PIc}}$ and $\mathbf{G_{del}}$ are the transfer function matrices of the current controller and the digital & PWM delay, and $\mathbf{Y_L}$ is the admittance matrix of the output filter.

Considering the effect of synchronization, the variables related to the Park transform and its inverse can be updated by

$$\begin{aligned} \Delta \mathbf{v_g^c} &= \mathbf{G_{PLL}^v} \Delta \mathbf{v_g^s} \\ \Delta \mathbf{i_L^c} &= \mathbf{G_{PLL}^i} \Delta \mathbf{v_g^s} + \Delta \mathbf{i_L^s} \\ \Delta \mathbf{d^s} &= -\mathbf{G_{PLL}^d} \Delta \mathbf{v_g^s} + \Delta \mathbf{d^c} \end{aligned} \tag{4}$$

where $\Delta \mathbf{d^c}$ and $\Delta \mathbf{d^s}$ are the duty cycle perturbations in synchronized-frame and system frame, $\mathbf{G_{PLL}^v}$, $\mathbf{G_{PLL}^i}$, and $\mathbf{G_{PLL}^d}$ define the relationship between the grid voltage perturbation in system frame and the grid voltage perturbation, the converter current perturbation, and the duty cycle perturbation in synchronized-frame. All the detailed matrices of the GFL converter are given in the Appendix.

Combining (2), (3) and (4), one can obtain the impedance matrix of the GFL converter, which is

$$\begin{aligned} \mathbf{Z_{GFL}} &= -\frac{\Delta \mathbf{v_g^s}}{\Delta \mathbf{i_L^s}} \\ &= (\mathbf{E_{2\times 2}} + \mathbf{Y_L G_{del} G_{PIc}}) \cdot (\mathbf{Y_L} + \mathbf{Y_L G_{PLL}^d} \\ &\quad - \mathbf{Y_L G_{del} G_{PLL}^v} + \mathbf{Y_L G_{del} G_{PIc} G_{PLL}^i})^{-1} \end{aligned} \tag{5}$$

where $\mathbf{E_{2\times 2}}$ is the identity matrix.

Based on the model of (5), the frequency responses of the impedance matrix of the GFL converter can be obtained and shown by the blue curves in Fig. 5. For comparison, the measured impedance using mono-frequency sweeping method is shown by the red circles in the same figure. The system parameters given in Table I are used in the model validation. Obviously, the frequency responses of the theoretical model

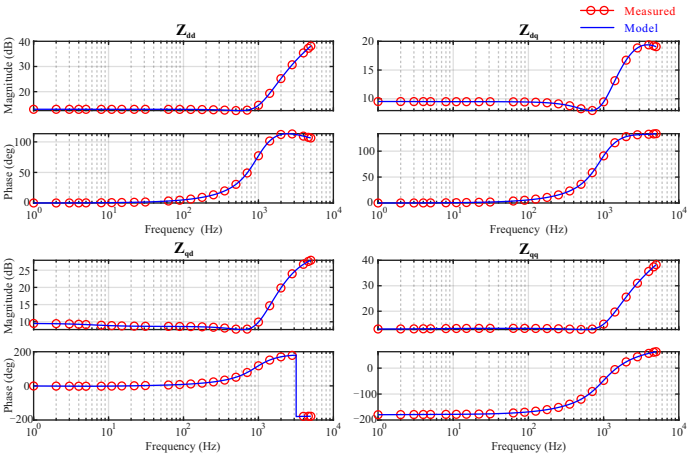

Fig. 5. Comparison of theoretical model (blue curves) and measured impedance (red circles) of GFL converter.

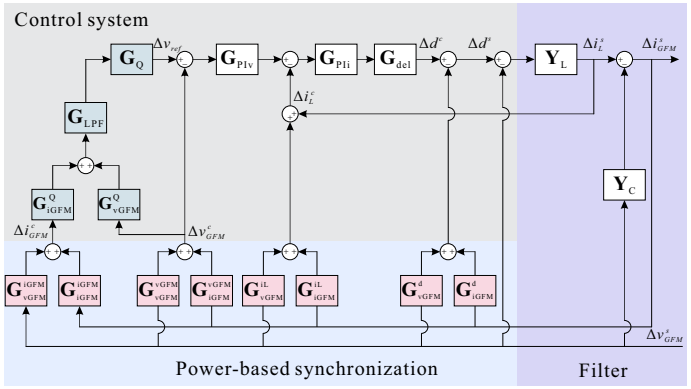

Fig. 6. Small-signal model of GFM converter considering the power-based synchronization

well match the measured impedance. It can be seen that the impedance of the diagonal elements (Z_{dd} and Z_{qq}) is relatively low in the low-frequency range, indicating the power loop as well as current loop in the dq frame can well track the fundamental component and alleviate low-order harmonics. Due to the PLL effect, the impedance profiles of the diagonal elements are asymmetric. Specifically, Z_{dd} in the low-frequency range behaves as a positive resistor, while a negative resistive characteristic can be observed in the low-frequency range of Z_{qq}, which could compromise the system stability [8], [9].

B. Grid-forming Converters

Based on the system configuration, the small-signal model of a GFM converter is shown in Fig. 6. The multiloop scheme with the voltage outer loop and the current inner loop in the dq frame is shown in gray area, while the control plant including filter is shown in purple area. The power control loop is highlighted by cyan blocks, while the effect of power-based synchronization is considered and represented by pink blocks.

According to Fig. 6, the small-signal model of control system can be described by

$$\Delta\mathbf{d^c} = \mathbf{G_{PIi}G_{del}}[-\Delta\mathbf{i_L^c} + \mathbf{G_{PIv}}(\Delta\mathbf{v_{ref}} - \Delta\mathbf{v_{GFM}^c})] \quad (6)$$

and the filter model is

$$\Delta\mathbf{i_{GFM}^s} = \mathbf{Y_L}\Delta\mathbf{d^s} - (\mathbf{Y_c} + \mathbf{Y_L})\Delta\mathbf{v_{GFM}^s} \quad (7)$$

Here, the superscripts ^{c} and ^{s} are used to indicate the variables related to the synchronization frame and the system frame, respectively. $\Delta\mathbf{d^c}$ and $\Delta\mathbf{d^s}$ are the duty cycle perturbations in synchronized-frame and system frame, $\Delta\mathbf{v_{GFM}^c}$ and $\Delta\mathbf{v_{GFM}^s}$ are the voltage perturbations in synchronized-frame and system frame, $\Delta\mathbf{i_L^c}$ is the inductor current perturbation in synchronized-frame, $\Delta\mathbf{i_{GFM}^s}$ is the current perturbation in system frame, $\mathbf{G_{PIi}}$, $\mathbf{G_{PIv}}$ and $\mathbf{G_{del}}$ are the transfer function matrices of the current controller, voltage controller, and the digital & PWM delay, $\mathbf{Y_L}$ and $\mathbf{Y_c}$ are the admittance matrices of the output LC filter.

When power-based synchronization being considered, the variables related to the Park transform and its inverse can be written by

$$\begin{aligned}
\Delta\mathbf{v_{GFM}^c} &= \mathbf{G_{vGFM}^{vGFM}}\Delta\mathbf{v_{GFM}^s} + \mathbf{G_{iGFM}^{vGFM}}\Delta\mathbf{i_{GFM}^s} \\
\Delta\mathbf{i_{GFM}^c} &= \mathbf{G_{vGFM}^{iGFM}}\Delta\mathbf{v_{GFM}^s} + \mathbf{G_{iGFM}^{iGFM}}\Delta\mathbf{i_{GFM}^s} \\
\Delta\mathbf{i_L^c} &= \mathbf{G_{vGFM}^{iL}}\Delta\mathbf{v_{GFM}^s} + \mathbf{G_{iGFM}^{iL}}\Delta\mathbf{i_{GFM}^s} + \Delta\mathbf{i_L^s} \\
\Delta\mathbf{d^s} &= -\mathbf{G_{vGFM}^{d}}\Delta\mathbf{v_{GFM}^s} - \mathbf{G_{iGFM}^{d}}\Delta\mathbf{i_{GFM}^s} + \Delta\mathbf{d^c}
\end{aligned} \quad (8)$$

where $\mathbf{G_{vGFM}^{vGFM}}$, $\mathbf{G_{vGFM}^{iGFM}}$, $\mathbf{G_{vGFM}^{iL}}$, $\mathbf{G_{vGFM}^{d}}$ define the responses from the GFM voltage perturbation in system frame to the voltage perturbation, the current perturbation, the inductor current perturbation, and the duty cycle perturbation in synchronized-frame, $\mathbf{G_{iGFM}^{vGFM}}$, $\mathbf{G_{iGFM}^{iGFM}}$, $\mathbf{G_{iGFM}^{iL}}$, $\mathbf{G_{iGFM}^{d}}$ define the responses from the GFM current perturbation in system frame to the voltage perturbation, the current perturbation, the inductor current perturbation, and the duty cycle perturbation in synchronized-frame. The detailed matrices are given in the Appendix. Combining (6), (7) and (8), one can obtain the impedance matrix of the GFM converter, which is illustrated in (9).

Based on the model of (9), the impedance matrix of the GFM converter is shown by the blue curves in Fig. 7. For comparison, the measured impedance is shown by the red circles in the same figure. The system parameters used in the model validation are listed in Table I. It can be seen that the theoretical model can well match the measured impedance. If the effect of power-based synchronization is neglected, the voltage amplitude and frequency are fixed with their nominal values. Under this circumstance, a simplified impedance matrix can be obtained and is shown by the green curves. Compared to the one with the power-based synchronization, it can be seen that the impedance profiles of the non-diagonal elements are modified. In particular, Z_{dq} in the low-frequency range is resistive without the effect of synchronization, while it behaves as a negative resistance when the power-based synchronization is used. The magnitude of the negative resistance is related to the inertia and the damping factor. In this regard,

$$\mathbf{Z_{GFM}} = [(\mathbf{Y}_L\mathbf{G}_{del}\mathbf{G}_{PIi}\mathbf{G}_{PIv})(\mathbf{G}_Q\mathbf{G}_{LPF}\mathbf{G}^{Q}_{vGFM}\mathbf{G}^{vGFM}_{vGFM} + \mathbf{G}_Q\mathbf{G}_{LPF}\mathbf{G}^{Q}_{iGFM}\mathbf{G}^{iGFM}_{vGFM} - \mathbf{G}^{vGFM}_{vGFM}) - (\mathbf{Y}_L\mathbf{G}_{del}\mathbf{G}_{PIi}\mathbf{G}^{iL}_{vGFM} + \mathbf{Y}_L) - \mathbf{Y}_C(\mathbf{E_{2\times 2}} + \mathbf{Y}_L\mathbf{G}_{del}\mathbf{G}_{PIi})]^{-1}[-\mathbf{Y}_L(\mathbf{G}_{del}\mathbf{G}_{PIi} + \mathbf{G}_{del}\mathbf{G}_{PIi}\mathbf{G}^{iL}_{iGFM} + \mathbf{G}^{d}_{iGFM}) - \mathbf{E_{2\times 2}} + \mathbf{Y}_L\mathbf{G}_{del}\mathbf{G}_{PIi}\mathbf{G}_{PIv} \cdot (\mathbf{G}_Q\mathbf{G}_{LPF}\mathbf{G}^{Q}_{vGFM}\mathbf{G}^{vGFM}_{iGFM} + \mathbf{G}_Q\mathbf{G}_{LPF}\mathbf{G}^{Q}_{iGFM}\mathbf{G}^{iGFM}_{iGFM} - \mathbf{G}^{vGFM}_{iGFM})] \tag{9}$$

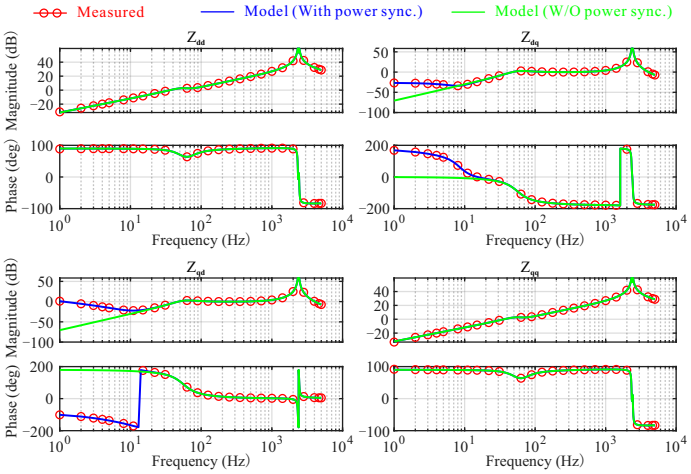

Fig. 7. Comparison of theoretical model (blue curves) and measured impedance (red circles) of GFM converter.

the parameters of the power-based synchronization must be well designed to avoid the potential oscillations.

IV. Interactions Between GFL and GFM Converters

Based on the developed models in the previous section, the stability of a two-bus system with GFL and GFM converters can be assessed by using the generalized Nyquist criterion [34], [35]. Considering the grid impedance, the impedance ratio or the minor loop of the system is given by

$$\mathbf{L} = \mathbf{Z_G} \cdot \mathbf{Y_{SEQ}} \tag{10}$$

where $\mathbf{Z_G}$ is the equivalent grid impedance matrix, and $\mathbf{Y_{SEQ}}$ is the equivalent admittance matrix seen from the PCC. The system stability can be predicted based on the frequency responses of the eigenvalues of the impedance ratio [10], which are

$$det\,[\lambda_i(s)\mathbf{E_{2\times 2}} - \mathbf{Z_G} \cdot \mathbf{Y_{SEQ}}] = 0 \tag{11}$$

The overall system is stable if and only if the eigenvalues (or the characteristic loci) $\lambda_i(s)$ satisfy the Nyquist criterion [34], [35].

The system configuration of the two-bus system is shown in Fig. 8, and different different scenarios with the line impedance are studied in the followings. The scenario of two GFL converters has been studied in [12] and thus it will not be discussed in this paper. Two scenarios will be investigated: 1) a GFL and a GFM converters are connected to the two buses, respectively; 2) two GFM converters are connected to the two buses. With the considerations of system representation, the equivalent impedance models of the two-bus system for the

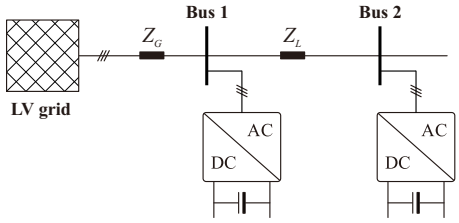

Fig. 8. System configuration of a two-bus system with power converters.

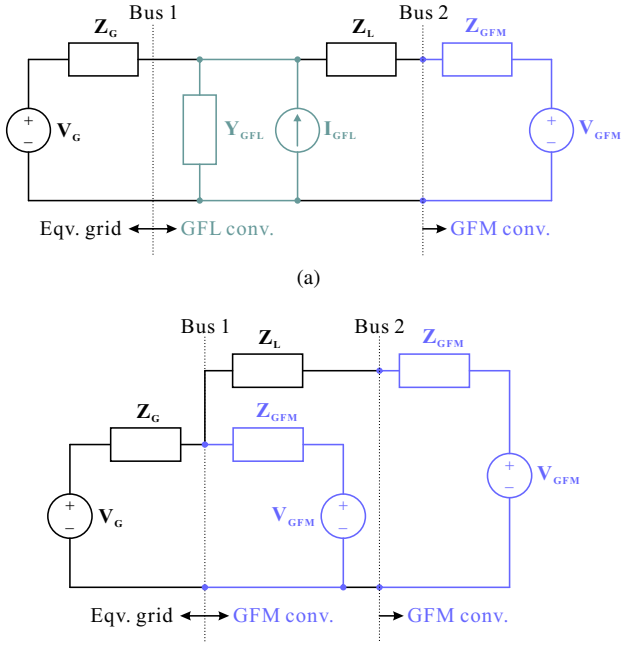

Fig. 9. Equivalent impedance models of two-bus system with power converters for different scenarios: (a) GFL and GFM converters and (b) two GFM converters.

two scenarios are given in Fig. 9. Here, $\mathbf{V_G}$ is the equivalent voltage source of the grid, $\mathbf{Z_L}$ is the equivalent line impedance between the two buses, $\mathbf{I_{GFL}}$ and $\mathbf{Y_{GFL}}$ are the equivalent current source and admittance of the GFL converter, $\mathbf{V_{GFM}}$ and $\mathbf{Z_{GFM}}$ are the equivalent voltage source and impedance of the GFM converter.

A. Scenario A: GFL and GFM Converters

In this scenario, a GFL converter connects to Bus 1 and a GFM converter connects to Bus 2. Based on the system configuration of Fig. 9a and (10), the minor loop can be obtained by

$$\mathbf{L_{A2}} = \frac{\mathbf{Z_{GFL}} \cdot (\mathbf{Z_{GFM}} + \mathbf{Z_L})}{\mathbf{Z_G} \cdot (\mathbf{Z_{GFL}} + \mathbf{Z_{GFM}} + \mathbf{Z_L})} \tag{12}$$

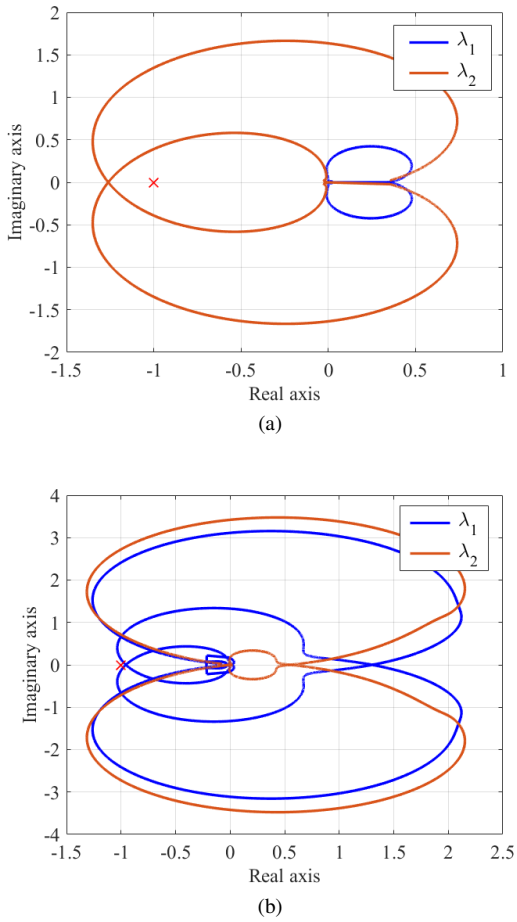

Fig. 10. Nyquist plots of two-bus system with power converters: (a) single GFL converter connects to Bus 1 and (b) GFL and GFM converters connect to Bus 1 and 2 respectively.

For comparison, the minor loop of a single GFL converter connects to Bus 1 is given by

$$\mathbf{L_{A1}} = \mathbf{Z_{GFL}} \cdot \mathbf{Z_G}^{-1} \tag{13}$$

In case of a weak grid, e.g., SCR is 3, applying the generalized Nyquist criterion to (13) and (12), the characteristic loci of the system are shown in Fig. 10a and Fig. 10b, respectively. It can be seen that one of the system characteristic loci (i.e., λ_2) encircles the critical point (-1, $j0$) when a GFL converter connects to the weak grid, and therefore the converter suffers from instability issue. However, when the GFM converter connects to Bus 2, it can be seen that none of the system characteristic loci encircles the critical point, showing the stability of the overall system is improved.

Since λ_2 is mainly influenced by the ratio of grid and converter impedance in qq axis, the frequency responses of the corresponding impedance are shown in Fig. 11a. In case of a single GFL converter, the equivalent imepdance Z_{qq} is illusrated by the red curve, which presents a negative resistive characteristic in the low-frequency range. When a GFM converter being connected, the characteristic in the low-frequency range can be modified, which turns out to be inductive. For this reason, the overall system is less likely to suffer from instability or oscillation caused by the low-frequency resonance. Moreover, when GFL being used alone, the crossover region between grid impedance and Z_{qq} is relatively wide, ranging from f_{cr1} to f_{cr2}. The phase difference between the two impedance falls into the unacceptable phase band [36], and thus causing stability issue at around $500\,\mathrm{Hz}$. When a GFM converter is connected to Bus 2, the magnitude of Z_{qq} in such a range can be modified and the crossover region can be largely reduced. It can be seen that the new crossover frequency f'_{cr1} moves rightwards, and under this circumstance the phase difference no longer falls into the unacceptable phase band.

The frequency responses of λ_2 for both cases are shown in Fig. 11b. In case of single GFL converter, a $-180°$ crossing can be identified at around $500\,\mathrm{Hz}$ when the magnitude is positive. For this reason, the overall system suffers from instability and sideband harmonics can be observed in the abc frame. When the GFM converter connects to Bus 2, both the magnitude and the phase of λ_2 are modified. In particular, the magnitude at the critical frequency can be reduced to be negative, leading to a stable system. Nevertheless, it is worth noting that the power-based synchronization and the filter of the GFM converter introduce two additional resonances as seen in the low- and the high-frequency ranges. Especially in the low-frequency range, as soon as the resonance exceeds $0\,\mathrm{dB}$, the $-180°$ crossing can lead to instability in terms of sub-synchronous oscillation.

In Fig. 12a, the root loci of the two bus system with GFL and GFM converter are presented, when varying the SCR of the grid. The SCR varies from 13 to 1 in this case study. It can be seen that a pair of conjugate poles at around $3100\,\mathrm{rad/s}$ (around $500\,\mathrm{Hz}$) are gradually moving from the left side to the right half plane when the SCR decreases. This phenomenon can be reflected by the critical region of Fig. 11b, where the magnitude would increase from negative value to positive when decreasing the SCR. On the other hand, a pair of conjugate poles at around $35\,\mathrm{rad/s}$ (around $6\,\mathrm{Hz}$) locate in the right half plane when the SCR is high. This is due to the effect of power-based synchronization and it can be reflected by the resonance in low-frequency range Fig. 11b. It indicates the power-based synchronization could incur instability when the grid is strong. By decreasing the SCR, the pair of poles are moving to the left side. Moreover, the pairs of conjugates poles in the high-frequency range introduced by the filter resonances are far away from the imaginary axis, showing they are insensitive to the SCR changes.

B. Scenario B: Two Grid-forming Converters

In this scenario, two GFM converters using the virtual synchronous machine concept are connected to the two buses. Based on the system configuration of Fig. 9b and (10), the minor loop can be obtained by

$$\mathbf{L_{B2}} = \frac{\mathbf{Z_{GFM}} \cdot (\mathbf{Z_{GFM}} + \mathbf{Z_L})}{\mathbf{Z_G} \cdot (2\mathbf{Z_{GFM}} + \mathbf{Z_L})} \tag{14}$$

For comparison, the minor loop of a single GFM converter connects to Bus 1 is given by

$$\mathbf{L_{B1}} = \mathbf{Z_{GFM}} \cdot \mathbf{Z_G}^{-1} \tag{15}$$

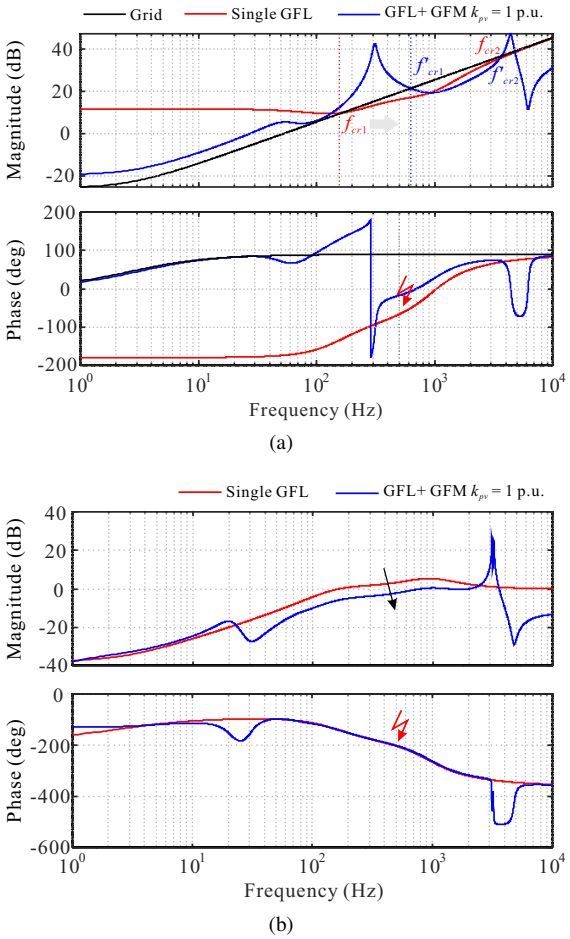

Fig. 11. Frequency responses of overall system of scenario A: (a) equivalent impedance of qq-axis and (b) eigenvalue λ_2.

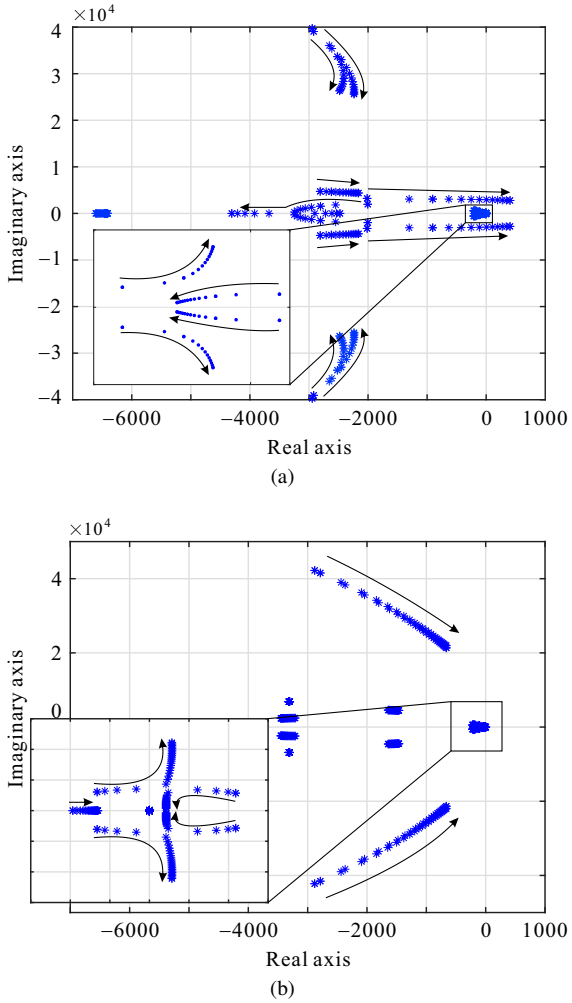

Fig. 12. Root loci of two-bus system with GFL and GFM converters when varying system parameters: (a) SCR and (b) line length.

In case of a strong grid, e.g., SCR is 10, applying the generalized Nyquist criterion to (14) and (15), the characteristic loci of the system are shown in Fig. 13a and Fig. 13b, respectively. In Fig. 13a, only one GFM converter connects to Bus 1 and none of the characteristic loci encircles the critical point. However, it can be seen in Fig. 13b that one of the system characteristic loci (i.e., λ_2) encircles the critical point (-1, $j0$) when two GFM converters connect to the two buses, and thus the grid suffers from instability issue.

The frequency responses of the converter impedance in qq axis in different conditions are shown in Fig. 14a. In case of a single GFM converter, as shown by the red curve, though the crossover region between grid impedance and Z_{qq} is relatively wide, the phase difference between the two impedance is small and can hardly fall into the unacceptable phase band. However, when another GFM converter being connected, the characteristic in the low-frequency range can be modified. A resonance is introduced in the low-frequency range as shown by the green curve. In the crossover region, the phase difference between the two impedance falls into the unacceptable phase band, and thus causing stability issue at around 2.3 Hz. Moreover, the connection of additional GFM converter leads the crossover region to become wider. The crossover frequency moves from f_{cr1} to f'_{cr1}, which could aggrevate the stability issue of low-frequency range. When the line length between the two converters increases, as shown by the blue curve, it can be seen that the resonance in the low-frequency is alleviated and the the crossover region can be reduced. The phase difference no longer falls into the unacceptable phase band and therefore the system becomes stable.

The frequency responses of λ_2 for different cases are shown in Fig. 14b. In case of single GFM converter, there is no $-180°$ crossing can be identified when the magnitude is positive. However, after the second GFM being connected to Bus 2, the $-180°$ crossing at the resonant frequency of 2.3 Hz can be identified, leading the overall system to be unstable. When the line length increases, both the resonance and the $-180°$ crossing are alleviated, and thus the system can maintain stability.

Nevertheless, it is worth noting that the line impedance between the two converters introduces a resonance and antiresonance in the high-frequency range. By increasing the length, this issue could be further exaggerated and lead to high-frequency oscillations. To better study the effect of line impedance on system stability, the root loci of two GFM converters when varying the length of the line are presented in Fig. 15. In this case study, the type of UG-02 is used and

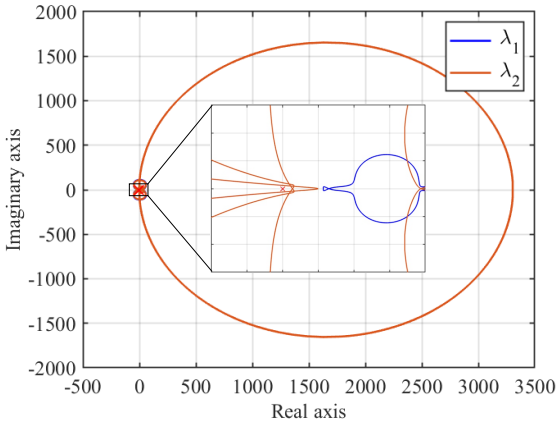

(a)

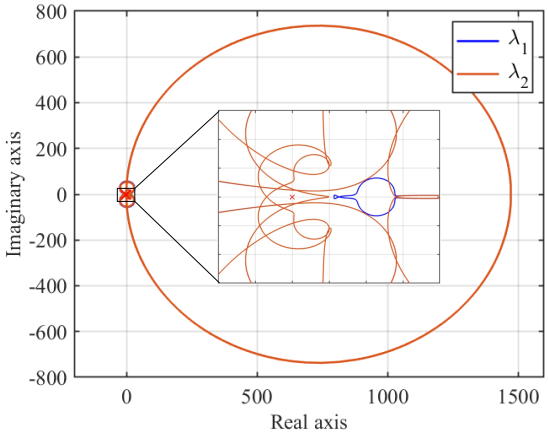

(b)

Fig. 13. Nyquist plots of two-bus system with power converters: (a) single GFM converter connects to Bus 1 and (b) two GFM converters connect to Bus 1 and 2.

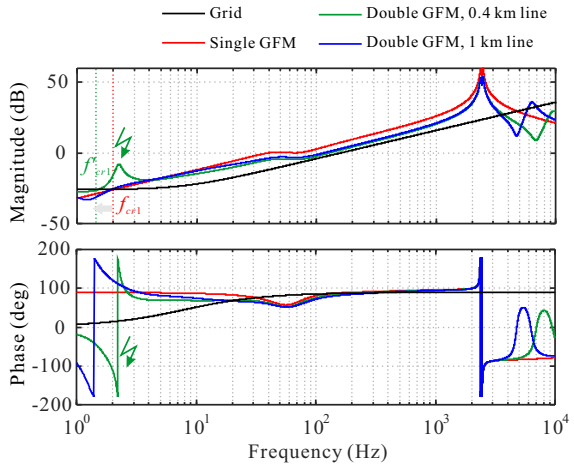

(a)

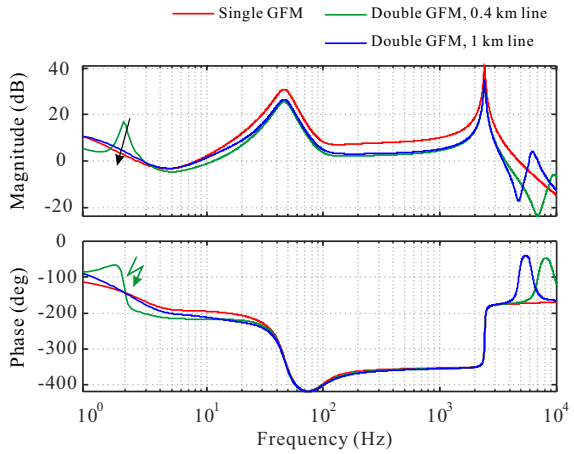

(b)

Fig. 14. Frequency responses of overall system of scenario B: (a) equivalent impedance of qq-axis and (b) eigenvalue λ_2.

the line length increases from 0 to 1.5 km. It can be seen that the poles in the high-frequency range are moving rightwards when increasing the line length. Nevertheless, the dominant poles in the low-frequency range locate on the right half plane when the line length is 0. By increasing the line length, the dominant poles can move from the right half plane to the left one, and thus the system becomes stable. This indicates the cable between the two GFM converters is necessary to maintain stability, especially when the grid is strong.

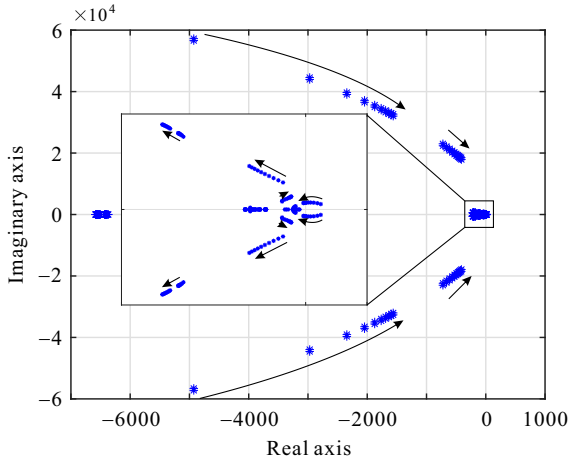

Fig. 15. Root loci of two-bus system with two GFM converters when varying line length.

V. Parameters Design For Stable Operation

In this section, the sensitivity of the dominant poles to different parameters in different scenarios are analyzed. Then, design guidelines of parameters of the two-bus system are presented based on their stable regions.

A. Scenario A: GFL and GFM Converters

To investigate the sensitivity of $\lambda_i(s)$ to the parameters, a Jacobian matrix J_a is defined as following:

$$J_a(\lambda_i) = \left[\frac{\partial \sigma_i}{\partial D_p}, \frac{\partial \sigma_i}{\partial J}, \frac{\partial \sigma_i}{\partial k_{pv}}, \frac{\partial \sigma_i}{\partial k_{pi}}, \frac{\partial \sigma_i}{\partial k_{iv}}, \frac{\partial \sigma_i}{\partial k_{ii}}, \frac{\partial \sigma_i}{\partial f_{res}}, \frac{\partial \sigma_i}{\partial k_{pc}}, \frac{\partial \sigma_i}{\partial k_{ic}}, \frac{\partial \sigma_i}{\partial k_{ppll}}, \frac{\partial \sigma_i}{\partial k_{ipll}}, \frac{\partial \sigma_i}{\partial SCR}\right]$$

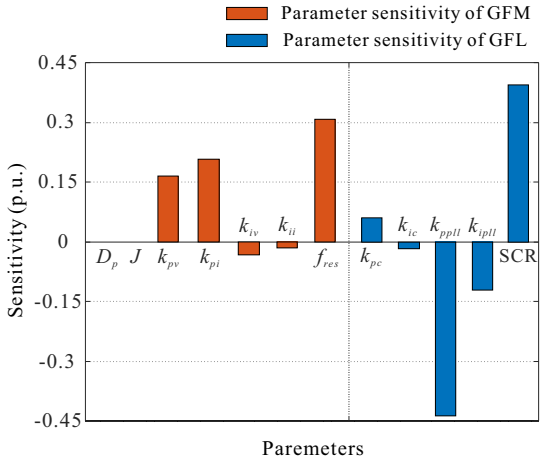

Fig. 16. Sensitivity analysis of the real part of the most critical poles to different parameters of scenario A.

where σ_i is the real part of the most critical or dominant poles of ith eigenvalue, D_p and J are the damping ratio and the virtual inertia of the GFM converter, k_{pv}, k_{iv}, k_{pi}, and k_{ii} are the PI control parameters of the GFM converter, f_{res} is the filter resonant frequency of the GFM converter, k_{pc} and k_{ic} are the PI control parameters of the GFL converter, k_{ppll} and k_{ipll} are the control parameters of the SRF-PLL.

The sensitivity analysis of the dominant poles to the variation of different parameters are given in Fig. 16. A bar with positive value shows a more stable condition (i.e., dominant poles move leftwards), whereas a negative one indicates the system tends to be less stable. According to the previous analysis, the system stability is mainly influenced by λ_2 and it can be seen that the dominant poles of λ_2 to the variations of k_{pv}, k_{pi}, and f_{res} of the GFM converter are positive and meanwhile the most influential. It indicates that the system stability can be improved by increasing of the three parameters of the GFM converter. Meanwhile, it can be seen that the PLL parameters of the GFL converter and the grid SCR also have importance effects on the stability. By increasing k_{ppll} and k_{ipll}, or reducing the SCR, the system stability can be compromised.

The stability regions of the two-bus system in scenario A when PLL bandwidth of GFL converter changing from 0.7 to 1.3 p.u. are shown in Fig. 17. The impacts of the three sensitive parameters of the GFM converter on the stability are studied. Here, the nominal values of the PLL bandwidth, k_{pv}, k_{pi}, and f_{res} are $200\,\mathrm{Hz}$, 2.0, 5.0, and $2000\,\mathrm{Hz}$. By increasing k_{pv}, k_{pi}, or f_{res} of LC filter of GFM converter, the system can become stable even the PLL bandwidth is relatively high. Moreover, the stability regions of the two-bus system when SCR changing from 1 to 9 are studied and shown in Fig. 18. Similar to Fig. 17, the original unstable system can become stable by increasing the parameters of GFM converter when the SCR is relatively low. Therefore, it can be concluded that larger k_{pv}, k_{pi}, and f_{res} can improve the stability of a two-bus system with GFL and GFM converters. By using the Robust Control Toolbox, k_{pv} and k_{pi} of $[0.5p.u., 1.0p.u.]$, f_{res} of $[0.6p.u., 0.9p.u.]$ are recommended so that the two-bus system with GFL and GFM converters can maintain stability and meanwhile have relatively high performance. Besides, the PLL bandwidth of the GFL converter must not exceed 1.2 p.u. (especially when SCR is lower than 3) according to the stability regions otherwise the connected GFM converter can no longer improve the system stability.

B. Scenario B: Two Grid-forming Converters

To analyze the sensitivity of $\lambda_i(s)$ to the parameters, the Jacobian matrix of scenario B J_b is defined by

$$J_b(\lambda_i) = \Big[\frac{\partial\sigma_i}{\partial J_{1/2}}, \frac{\partial\sigma_i}{\partial Dp_{1/2}}, \frac{\partial\sigma_i}{\partial k_{pv1/2}}, \frac{\partial\sigma_i}{\partial k_{iv1/2}}, \frac{\partial\sigma_i}{\partial k_{pi1/2}}, \frac{\partial\sigma_i}{\partial k_{ii1/2}}, \frac{\partial\sigma_i}{\partial f_{res1/2}}, \frac{\partial\sigma_i}{\partial R_{line}}, \frac{\partial\sigma_i}{\partial X_{line}}\Big] \tag{17}$$

where D_p and J are the damping ratio and virtual inertia of the GFM converters, the subscripts 1 and 2 represent the GFM converters at Bus 1 and 2, R_{line} and X_{line} are the resistance and reactance of the cable between two buses. The sensitivity analysis of the dominant poles to the variation of different parameters are given in Fig. 19. It can be seen that the dominant poles (or system stability) are mainly influenced by five parameters, which are D_{p1}, J_1, k_{iv1} of the GFM converter at Bus 1, and the line parameters R_{line} and X_{line}. This indicates that the system stability is determined by the control parameters of the GFM converter at Bus 1 and the line impedance, while the rest of the parameters have minor impacts on the stability of the overall system.

The stability regions of the two-bus system in scenario B when SCR changing from 2 to 10 are shown in Fig. 20. The influences of the three sensitive control parameters of GFM converter at Bus 1 on the system stability are studied. Here, the nominal values of D_{p1}, J_1, k_{iv1} are 120, 5.0, and 500, respectively. It can be seen that the overall system becomes unstable when the grid getting stronger (SCR getting higher). By increasing D_{p1} and k_{iv1}, or reducing J_1 of GFM converter at Bus 1, the stability of the overall system can be improved for different grid representations. In particular, D_{p1} plays a major role: it allows the system to maintain stability even the SCR equals to 10. Then, the stability regions of the two-bus system when the line length between two converters changing from 0.3 to $1.3\,\mathrm{km}$ are investigated and shown in Fig. 21. Obviously, the unstable system can turn into a stable one by increasing the line length. Especially when the line length exceeds $0.65\,\mathrm{km}$, meanwhile the control parameters are well designed, the overall system can always maintain stability according to the regions. For a system with short line, the original unstable system can also become stable by turning the parameters of GFM converter at Bus 1: increasing D_{p1} and k_{iv1}, or reducing J_1. By using the Robust Control Toolbox, D_{p1} of $[0.6p.u., 1.0p.u.]$, J_1 of $[0.15p.u., 0.35p.u.]$, k_{iv1}, of $[0.5p.u., 1.0p.u.]$ are recommended so that the two-bus system with two GFM converters can maintain stability and meanwhile have relatively high performance. Besides, take UG-02 cable as an example, the line length is suggested to be longer than $0.35\,\mathrm{km}$ according to the stability regions

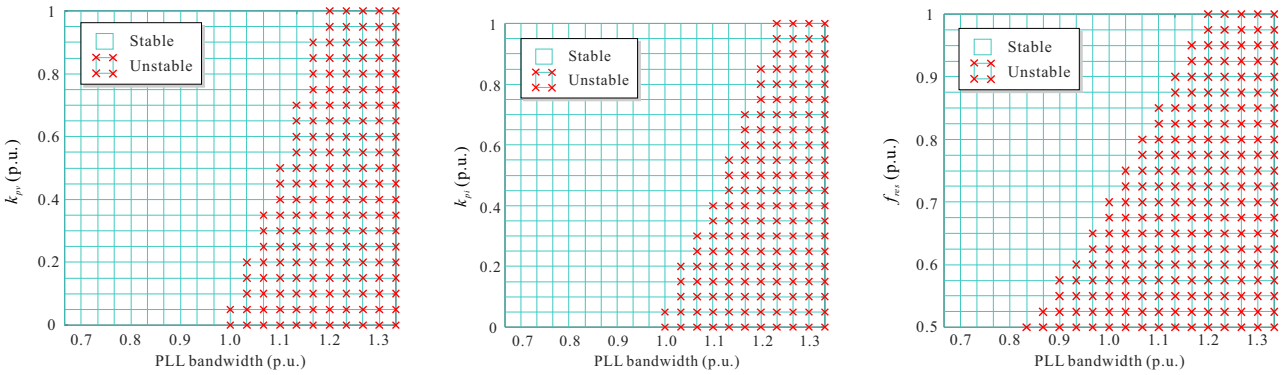

Fig. 17. Stability regions of two-bus system in scenario A when PLL bandwidth of GFL converter changing from 0.7 p.u. to 1.3 p.u.: (a) variation of k_{pv}, (b) variation of k_{pi}, and (c) variation of f_{res} of GFM converter.

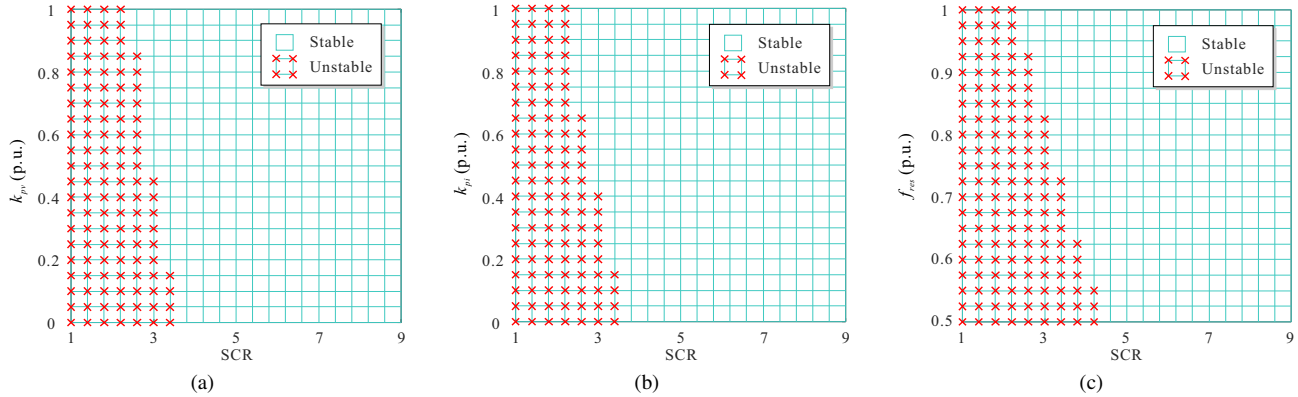

Fig. 18. Stability regions of two-bus system in scenario A when SCR changing from 1 to 9: (a) variation of k_{pv}, (b) variation of k_{pi}, and (c) variation of f_{res} of GFM converter.

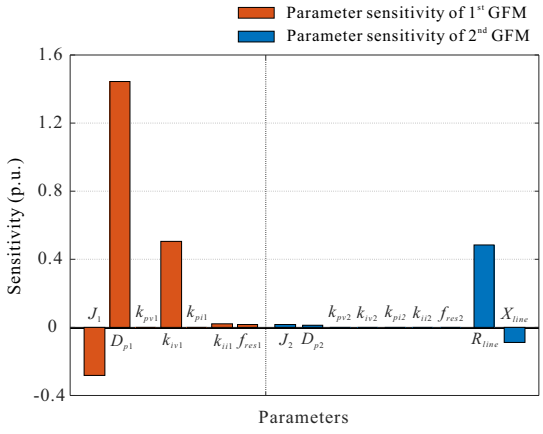

Fig. 19. Sensitivity analysis of the real part of the most critical poles to different parameters of scenario B.

otherwise the system stability can no longer be improved by tuning the control parameters in a strong grid.

VI. Filter-based Stabilized Control of GFM Converters

According to Fig. 10 and Fig. 13, the interactions between the two converters could incur instability. The critical points could appear either in low-frequency range (e.g., Scenario B) or in high-frequency range (e.g., Scenario A). To solve the potential stability issue, a stabilized control strategy based on the digital Biquad filter will be proposed for the GFM converter.

The generic transfer function of Biquad filter can be expressed by

$$G_{Bi} = \frac{s^2 + 2D_z\omega_z s + \omega_z^2}{s^2 + 2D_p\omega_p s + \omega_p^2} \tag{18}$$

which contains two poles and two zeros. Here, ω_z and ω_p are the frequencies of the poles and zeros, the deepness and wideness of the filter will be determined by the two damping coefficients D_z and D_p, respectively.

In general, both the magnitude and the phase at the critical point can be modified by means of Biquad filter, and eventually alters the phase margin of the overall system. To mitigate instability, the frequency of the zeros ω_z can be set at the critical frequency so that the magnitude at the critical point yields to be negative. Meanwhile, the frequency of the poles ω_p is expected to be in the stable region. In this regard, the introduced poles of Biquad filter will not aggravate the situation.

The schematic diagram of the proposed filter-based stabilized control is shown in Fig. 22, where the Biquad filter is

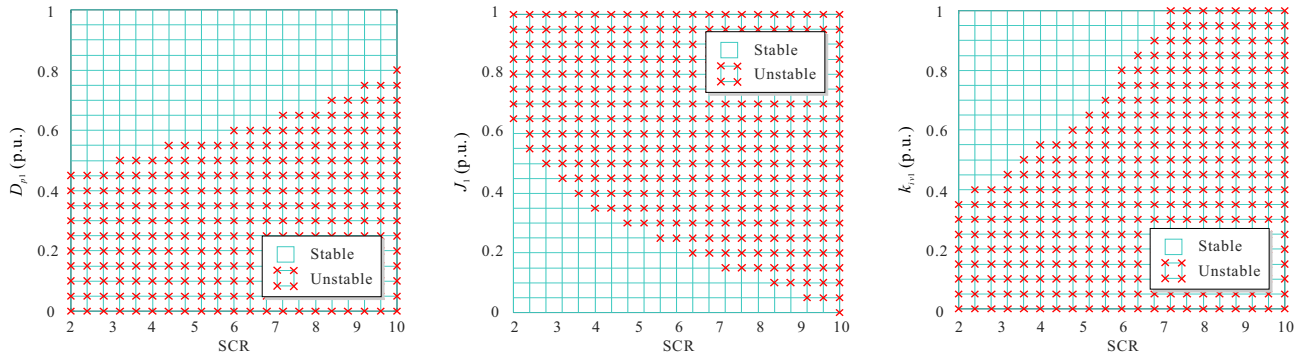

Fig. 20. Stability regions of two-bus system in scenario B when SCR changing from 2 to 10: (a) variation of D_{p1}, (b) variation of J_1, and (c) variation of k_{iv1} of GFM converter at Bus 1.

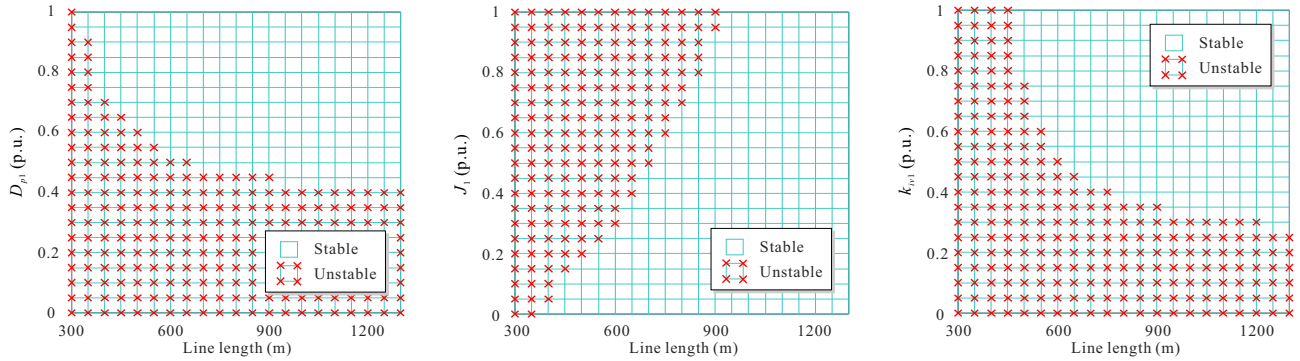

Fig. 21. Stability regions of two-bus system in scenario B when line length changing from 0.3 to 1.3 km: (a) variation of D_{p1}, (b) variation of J_1, and (c) variation of k_{iv1} of GFM converter at Bus 1.

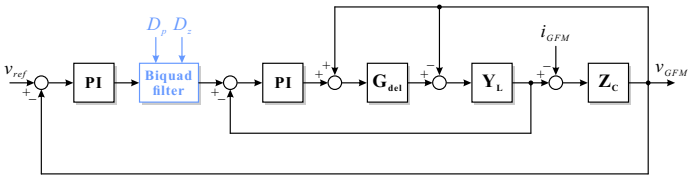

Fig. 22. Schematic diagram of the proposed filter-based stabilized control strategy for GFM converters.

plugged into the voltage outer loop of the GFM converter. By considering the effect of Biquad filter, using the generalized modeling procedure, the model of control system can be updated by

$$\Delta \mathbf{d}^{\mathbf{c}}_{\mathbf{Biquad}} = \mathbf{G_{PIi}G_{del}}[-\Delta \mathbf{i}^{\mathbf{c}}_{\mathbf{L}} + \mathbf{G_{PIv}G_{Bi}}(\Delta \mathbf{v_{ref}} - \Delta \mathbf{v}^{\mathbf{c}}_{\mathbf{GFM}})] \tag{19}$$

The rest models including the filter model and the synchronization model remain the same. Combining (7), (8), and (19), the updated impedance matrix of the GFM with the filter-based stabilized control strategy can be obtained.

Using the updated GFM impedance matrix, the stability of the two-bus system under scenario A and B can be reassessed. The frequency responses of λ_2 of the two scenarios with the filter-based stabilized control are shown in Fig. 23. In both case studies, the system and control parameters used in the previous section have been taken into account. For scenario A, though the overall system is stable initially, the magnitude of λ_2 can be reduced when the Biquad filter being implemented as shown in Fig. 23a. This indicates the gain margin of the overall system can be improved, establishing higher robustness. In case of two GFM converters, the overall system is unstable initially, while it becomes stable when using the Biquad filter as shown in Fig. 23b. It can be seen that both magnitude and phase of λ_2 at the critical point have been modified to be a more stable manner.

With the inclusion of the Biquad filter, the frequency responses of the eigenvalues around ω_z and ω_p turns out:

$$\begin{aligned} &\angle\lambda_{1,2}(s)_{s\approx j\omega_z} > -180(\text{deg}) \quad \text{if}\,|\lambda_{1,2}(s)|_{s\approx j\omega_z} > 1(0\,\text{dB}) \\ &|\lambda_{1,2}(s)|_{s\approx j\omega_p} < 1 \quad \text{if}\angle\lambda_{1,2}(s)_{s\approx j\omega_p} < -180(\text{deg}) \end{aligned} \tag{20}$$

It is worth noting that criterion regarding the phase at the critical point (or ω_z) can only guarantee the stability under the ideal circumstance. Due to the introduced poles, the magnitude at the frequency of poles must fulfill the requirements of (20) to avoid new stability issue arisen.

The proposed filter-based stabilized control can also be extended to other "white-box" systems with converters. Provided the impedance models of the systems are known, the zeros and poles of the Biquad filter can be allocated to reshape the

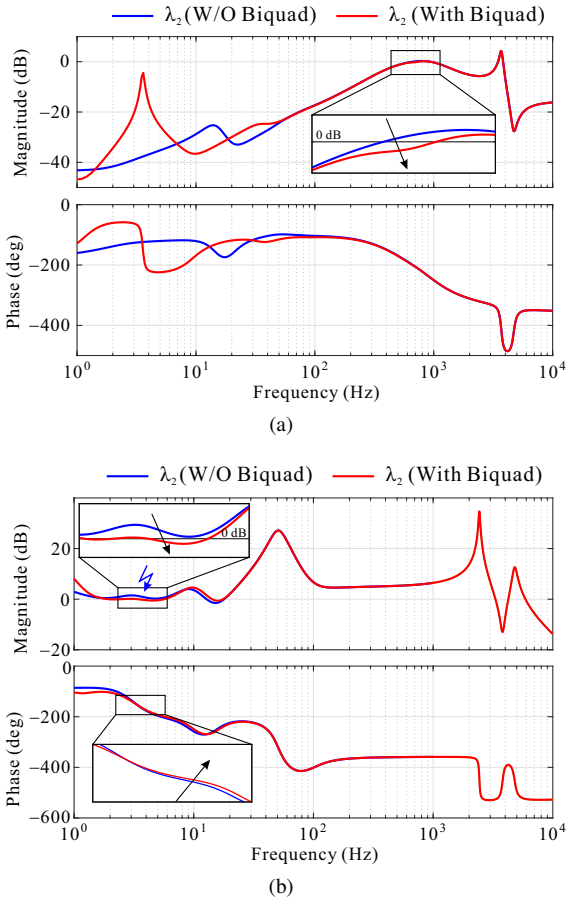

Fig. 23. Frequency responses of λ_2 of two scenarios using the proposed control: (a) GFL and GFM converters, and (b) two GFM converters.

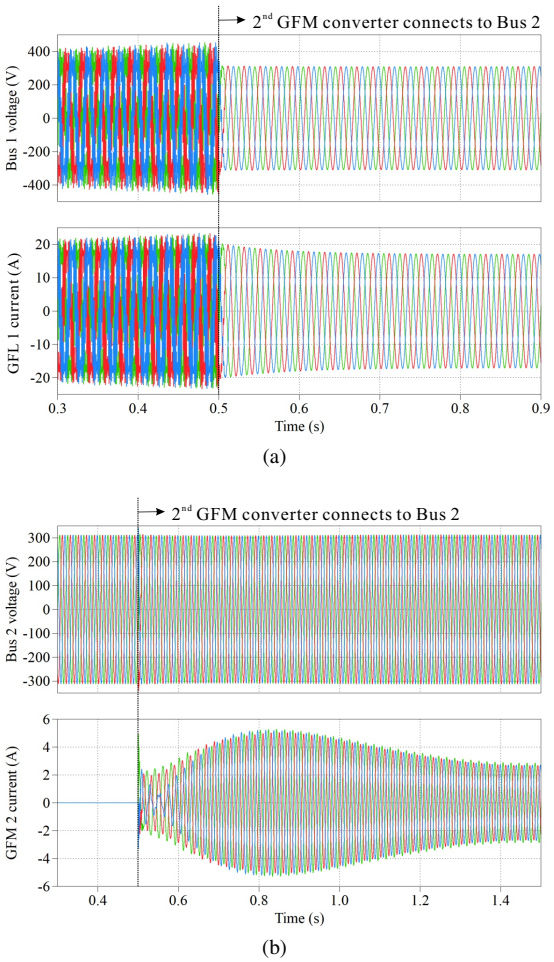

Fig. 24. Simulation results of two-bus system with GFL and GFM converters: (a) Bus 1 voltage and GFL converter current, and (b) Bus 2 voltage and GFM converter current.

converters' impedance, and therefore modifying the frequency responses of the critical eigenvalue as well as the stability margins. The design-oriented analysis can be used to well design the control parameters of the Biquad filter so that maintain system stability under different circumstances.

VII. Simulation and Experimental Results

In this section, the theoretical analysis and the proposed control strategy will be validated by simulation and experimental results.

A. Simulation Results

Firstly, the stability of the two-bus system with a GFL and a GFM converters is tested and its simulation results are shown in Fig. 24. The SCR of the grid is 3 in this case study, the PLL bandwidth of the GFL converter is 330 Hz and the power injection is 7.9 kW. If only a GFL converter connects to Bus 1, according to Fig. 24a, the system is unstable where the voltage and the current as well as the power are oscillating. At 0.5 s, the GFM converter connects to Bus 2. It can be seen that the waveforms of the GFL converter stop oscillating as soon as the GFM converter being integrated with the grid.

Secondly, the stability of the two-bus system with two GFM converters is tested and its simulation results are shown in Fig. 25. The SCR of the grid is 10 in this case study, and the active power setpoint of each converter is 2.5 kW. A GFM converter initially connects to Bus 1, at 2 s the second GFM converter connects to Bus 2. According to Fig. 25, the system becomes unstable as soon as the second GFM converter connects to Bus 2. It can be seen that the waveforms of the current and the power are oscillating in a low-frequency manner.

To remove the low-frequency oscillation, a cable with 1.5 mH impedance is connected between Bus 1 and 2. The corresponding waveforms are shown in Fig. 26. Likewise the previous case study, the SCR of the grid is 10 and the active power setpoint of each converter is 2.5 kW. However, the system can remain stability even the second GFM converter being integrated with the grid according to Fig. 26. Comparing to Fig. 25, the line impedance between the two buses improves the stability of the two-bus system with two GFM converters.

Then, the proposed stabilized control strategy is verified in the two-bus system with two GFM converters and its simulation results are shown in Fig. 27. The SCR of the grid is 10 in this case study, and the active power setpoint of each converter is 2.5 kW. It can be seen that the system is unstable initially. At 3 s, the proposed stabilized control strategy based on the Biquad filter has been implemented in

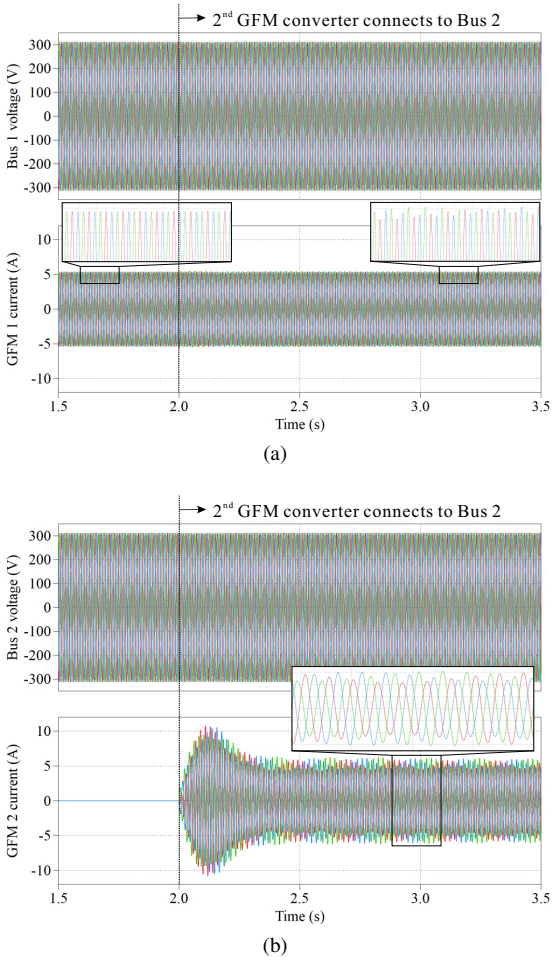

Fig. 25. Simulation results of two GFM converters without cable between two buses: (a) Bus 1 voltage and GFM converter current, and (b) Bus 2 voltage and GFM converter current.

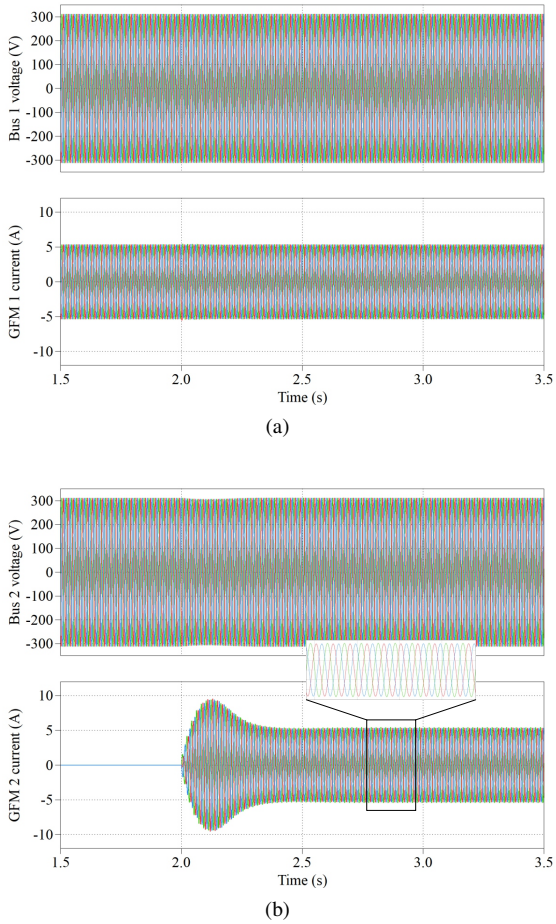

Fig. 26. Simulation results of two GFM converters with cable between two buses: (a) Bus 1 voltage and GFM converter current, and (b) Bus 2 voltage and GFM converter current.

the GFM converter connecting to Bus 2. After one cycle, the system becomes stable since the waveforms of the bus voltage and converter current stop oscillation and with relatively high power quality.

B. Experimental Results

To verify the effectiveness of the theoretical analysis, experimental validations have been done in a laboratory setup. The system configuration of Fig. 8 is developed, where two Danfoss VLT AutomationDrive FC 302 converters are used for the power converters. The control strategies of Fig. 1 and Fig. 2 are employed for the GFL and GFM converters. The control algorithms are implemented by a real-time control system based on TI's digital signal processor.

Firstly, the stability of the two-bus system with GFL and GFM converters are studied experimentally. Initially, a single GFL converter connects to Bus 1 and its power injection is 2.5 kW. The SCR is 3 and the PLL bandwidth is tuned to be 530 Hz. This leads to the instability and it can be found in Fig. 28a that both the Bus 1 voltage and the current of the GFL converter oscillate. Then, a GFM converter connects to Bus 2 with power injection of 0.5 kW. It can be seen in Fig. 28b that the overall system can achieve stable operation when both GFL and GFM converters connect to the grid.

Then, the effectiveness of the proposed control strategy is validated by experiments. In the beginning, two GFM converters are connected to the two buses and the line impedance between the buses is 0.5 mH. The SCR is 6.5 and the power injection of each converter is 2.4 kW. The overall system is unstable as it can be seen in Fig. 29a since the current of both GFM converters are oscillating. The spectrum of the converter current is shown in Fig. 29b and the oscillating contents in the low-frequency range (around 7 Hz) can be identified. As soon as the proposed control being utilized, the overall system becomes stable as shown in Fig. 29c. Seen from the time-domain waveforms and the spectrum in Fig. 29d, the oscillations in the low-frequency range have been alleviated by using the proposed control strategy.

VIII. Conclusion

This paper studies the stability issues of a two-bus system with GFL and GFM converters. To well illustrate the problem, a generalized modeling procedure for both types of converters has been presented. Based on the models, the stability of the system and the interactions between the converters have been investigated. It shows that the stability of a weak grid

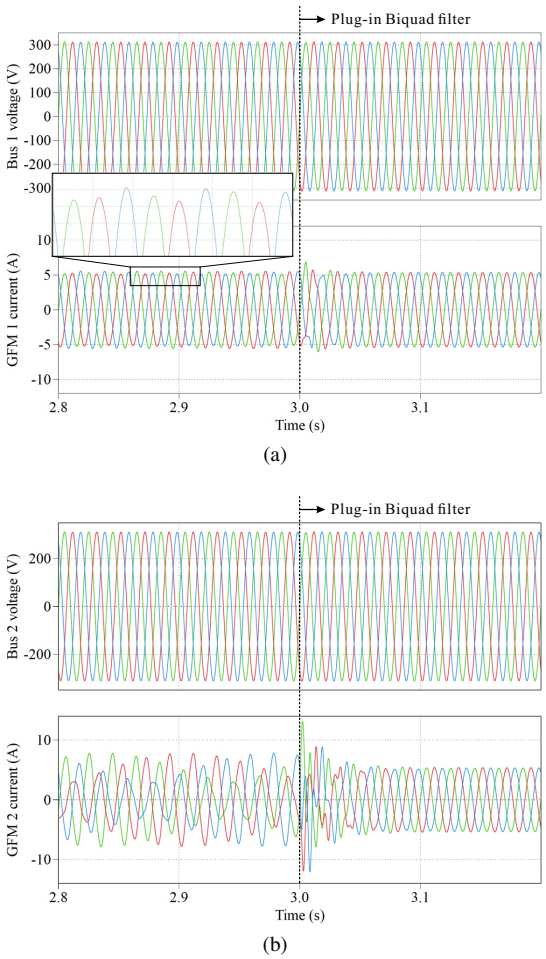

Fig. 27. Simulation results of two GFM converters with the proposed stabilized control: (a) Bus 1 voltage and GFM converter current, and (b) Bus 2 voltage and GFM converter current.

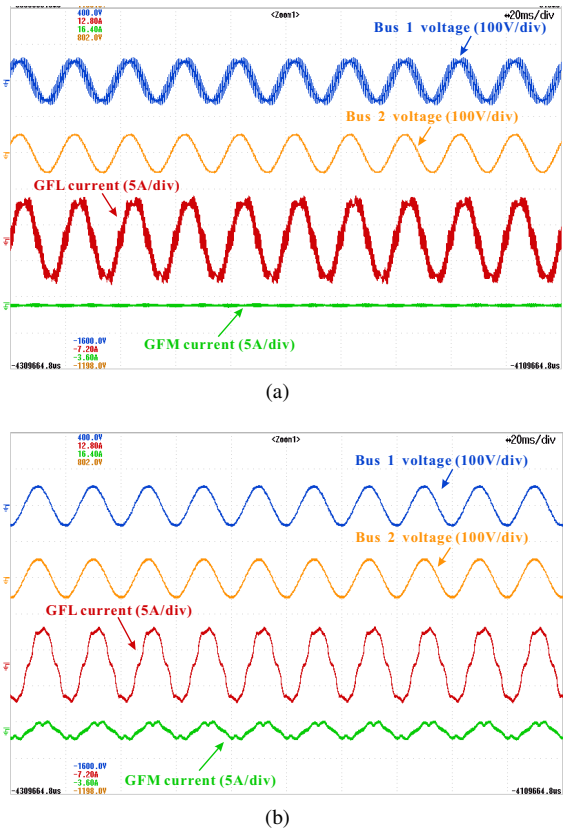

Fig. 28. Experimental results of a two-bus system when: (a) a single GFL converter connects to Bus 1 and (b) GFL and GFM converters connect to Bus 1 and 2 respectively.

with GFL converters can be improved by connecting GFM converters in the network. Moreover, a strong grid with GFM converters and low network impedance is likely to suffer from low-frequency oscillations (e.g., subsynchronous oscillation). The parameters sensitivity analysis of the two scenarios have been done and the stability regions of different parameters have been presented in order to provide design guidelines or parameters ranges for stable operation. To mitigate the oscillation, a stabilized control strategy based on the Biquad filter is proposed for the GFM converters. The simulation and experimental results have validated the effectiveness of the analysis and the proposed control.

APPENDIX

For the GFL converters, $\mathbf{G^{v}_{PLL}}$, $\mathbf{G^{i}_{PLL}}$, and $\mathbf{G^{d}_{PLL}}$ define the relationship between the grid voltage perturbation in system frame and the grid voltage perturbation, the converter current perturbation, and the duty cycle perturbation in synchronized-frame, the mathematical expressions of the transfer function matrices are

$$\mathbf{G}^{\mathrm{v}}_{\mathrm{PLL}} = \begin{bmatrix} 1 & V_{gq}G_{PLL} \\ 0 & 1 - V_{gd}G_{PLL} \end{bmatrix} \tag{21}$$

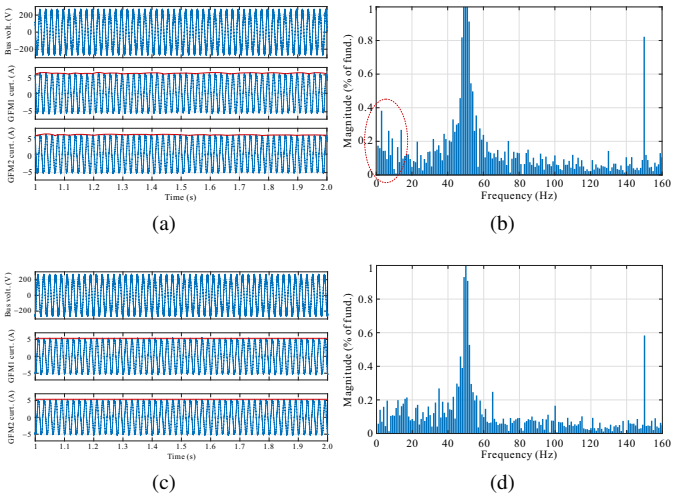

Fig. 29. Experimental results of two GFM converters with the proposed control: (a) waveforms of GFM converters without Biquad filter, (b) spectrum of GFM converter current without Biquad filter, (c) waveforms of GFM converters with Biquad filter, and (b) spectrum of GFM converter current with Biquad filter.

$$\mathbf{G}_{\mathrm{PLL}}^{\mathrm{i}}=\left[\begin{array}{cc}0 & I_{gq}G_{PLL}\\ 0 & -I_{gd}G_{PLL}\end{array}\right] \tag{22}$$

$$\mathbf{G}_{\mathrm{PLL}}^{\mathrm{d}}=\left[\begin{array}{cc}0 & -D_{q}G_{PLL}\\ 0 & D_{d}G_{PLL}\end{array}\right] \tag{23}$$

where V_{gd} and V_{gq} are the dc quantities of the grid voltage in dq frame, I_{gd} and I_{gq} are the dc quantities of the grid current in dq frame, D_d and D_q are the dc quantities of the averaged duty cycles in dq frame.

Here, the detailed expression of G_{PLL} is

$$G_{PLL}=\frac{sk_{ppll}}{s^{2}+sV_{gd}k_{ppll}+V_{gd}k_{ipll}} \tag{24}$$

where k_{ppll} and k_{ipll} are the proportional and the integral gains of the SRF-PLL.

In addition, $\mathbf{G_{PQ}}$, $\mathbf{G_{PIc}}$, and $\mathbf{G_{del}}$ are the transfer function matrices of the power control loop, current controller, and the digital & PWM delay, which can be expressed by

$$\mathbf{G}_{\mathrm{PQ}}=\left[\begin{array}{cc}-\frac{I_{dref}}{V_{gd}} & 0\\ -\frac{I_{qref}}{V_{gd}} & 0\end{array}\right] \tag{25}$$

$$\mathbf{G}_{\mathrm{PIc}}=\left[\begin{array}{cc}k_{pc}+\frac{k_{ic}}{s} & 0\\ 0 & k_{pc}+\frac{k_{ic}}{s}\end{array}\right] \tag{26}$$

$$\mathbf{G}_{\mathrm{del}}=\left[\begin{array}{cc}\frac{1}{1+1.5T_{s}s} & 0\\ 0 & \frac{1}{1+1.5T_{s}s}\end{array}\right] \tag{27}$$

where I_{dref} and I_{qref} are the current references in dq frame, k_{pc} and k_{ic} are the proportional and the integral gains of the current controller, T_s is the sampling interval.

The filter admittance $\mathbf{Y_L}$ is

$$\mathbf{Y}_{\mathrm{L}}=\frac{1}{L_{f}\left(s^{2}+\omega\right)^{2}}\left[\begin{array}{cc}s & \omega\\ -\omega & s\end{array}\right] \tag{28}$$

where L_f is the filter inductance, it can be expressed by $L_{f1}+L_{f2}$ if an LCL filter is used.

For the GFM converter, $\mathbf{G_{vGFM}^{vGFM}}$, $\mathbf{G_{vGFM}^{iGFM}}$, $\mathbf{G_{vGFM}^{iL}}$, $\mathbf{G_{vGFM}^{d}}$ define the responses from the GFM voltage perturbation in system frame to the voltage perturbation, the current perturbation, the inductor current perturbation, and the duty cycle perturbation in synchronized-frame, the mathematical expressions of the transfer function matrices are

$$\mathbf{G}_{\mathrm{vGFM}}^{\mathrm{vGFM}}=\left[\begin{array}{cc}1-aV_{GFMq}I_{GFMd} & -aV_{GFMq}I_{GFMq}\\ aV_{GFMd}I_{GFMd} & 1+aV_{GFMd}I_{GFMq}\end{array}\right] \tag{29}$$

$$\mathbf{G}_{\mathrm{vGFM}}^{\mathrm{iGFM}}=\left[\begin{array}{cc}-aI_{GFMd}I_{GFMq} & -aI_{GFMq}I_{GFMq}\\ aI_{GFMd}I_{GFMd} & aI_{GFMd}I_{GFMq}\end{array}\right] \tag{30}$$

$$\mathbf{G}_{\mathrm{vGFM}}^{\mathrm{iL}}=\left[\begin{array}{cc}-aI_{GFMd}I_{Lq} & -aI_{GFMq}I_{Lq}\\ aI_{GFMd}I_{Ld} & aI_{GFMd}I_{Lq}\end{array}\right] \tag{31}$$

$$\mathbf{G}_{\mathrm{vGFM}}^{\mathrm{d}}=\left[\begin{array}{cc}-aI_{GFMd}D_{q} & -aI_{GFMq}D_{q}\\ aI_{GFMd}D_{d} & aI_{GFMd}D_{d}\end{array}\right] \tag{32}$$

where V_{GFMd} and V_{GFMq} are the dc quantities of the output voltage in dq frame, I_{GFMd} and I_{GFMq} are the dc quantities of the output current in dq frame, I_{Ld} and I_{Lq} are the dc quantities of the inductor current in dq frame.

In addition, $\mathbf{G_{iGFM}^{vGFM}}$, $\mathbf{G_{iGFM}^{iGFM}}$, $\mathbf{G_{iGFM}^{iL}}$, $\mathbf{G_{iGFM}^{d}}$ define the responses from the GFM current perturbation in system frame to the voltage perturbation, the current perturbation, the inductor current perturbation, and the duty cycle perturbation in synchronized-frame, the mathematical expressions of the transfer function matrices are

$$\mathbf{G}_{\mathrm{iGFM}}^{\mathrm{vGFM}}=\left[\begin{array}{cc}1-aV_{GFMq}V_{GFMd} & -aV_{GFMq}V_{GFMq}\\ aV_{GFMd}V_{GFMd} & 1+aV_{GFMd}V_{GFMq}\end{array}\right] \tag{33}$$

$$\mathbf{G}_{\mathrm{iGFM}}^{\mathrm{iGFM}}=\left[\begin{array}{cc}1-aV_{GFMd}I_{GFMq} & -aV_{GFMq}I_{GFMq}\\ aV_{GFMd}I_{GFMd} & 1+aV_{GFMq}I_{GFMd}\end{array}\right] \tag{34}$$

$$\mathbf{G}_{\mathrm{iGFM}}^{\mathrm{iL}}=\left[\begin{array}{cc}-aV_{GFMd}I_{Lq} & -aV_{GFMq}I_{Lq}\\ aV_{GFMd}I_{Ld} & aV_{GFMq}I_{Ld}\end{array}\right] \tag{35}$$

$$\mathbf{G}_{\mathrm{iGFM}}^{\mathrm{d}}=\left[\begin{array}{cc}-aV_{GFMd}D_{q} & -aV_{GFMq}D_{q}\\ aV_{GFMd}D_{d} & aV_{GFMq}D_{d}\end{array}\right] \tag{36}$$

Here, the expression of coefficient a is

$$a=\frac{3}{2\omega_{0}\left(D_{p}+J_{S}\right)s} \tag{37}$$

where D_p and J are the damping factor and the virtual inertia.

$\mathbf{G_{PIv}}$, and $\mathbf{G_{PIi}}$ are the transfer function matrices of the voltage and current controller, which can be expressed by

$$\mathbf{G}_{\mathrm{PIv}}=\left[\begin{array}{cc}k_{pv}+\frac{k_{iv}}{s} & 0\\ 0 & k_{pv}+\frac{k_{iv}}{s}\end{array}\right] \tag{38}$$

$$\mathbf{G}_{\mathrm{PIi}}=\left[\begin{array}{cc}k_{pi}+\frac{k_{ii}}{s} & 0\\ 0 & k_{pi}+\frac{k_{ii}}{s}\end{array}\right] \tag{39}$$

where k_{pv} and k_{iv} are the proportional and the integral gains of the voltage outer loop controller, k_{pi} and k_{ii} are the proportional and the integral gains of the current inner loop controller.

$\mathbf{G}_{\mathrm{vGFM}}^{\mathrm{Q}}$ and $\mathbf{G}_{\mathrm{iGFM}}^{\mathrm{Q}}$ define the responses from the GFM voltage and current perturbations in system frame to the reactive power perturbation, which are

$$\mathbf{G}_{\mathrm{vGFM}}^{\mathrm{Q}}=\frac{3}{2}\left[\begin{array}{cc}-I_{GFMq} & I_{GFMd}\\ 0 & 0\end{array}\right] \tag{40}$$

$$\mathbf{G}_{\mathrm{iGFM}}^{\mathrm{Q}}=\frac{3}{2}\left[\begin{array}{cc}V_{GFMq} & -V_{GFMd}\\ 0 & 0\end{array}\right] \tag{41}$$

and $\mathbf{Q}$, and $\mathbf{G_{LPF}}$ are the transfer function matrices of the power controller and the low-pass filter, which can be expressed by

$$\mathbf{G}_{\mathrm{Q}}=\left[\begin{array}{cc}-K_{q} & 0\\ 0 & 0\end{array}\right] \tag{42}$$

$$\mathbf{G}_{\mathrm{LPF}}=\left[\begin{array}{cc}\frac{\omega_{f}}{s+\omega_{f}} & 0\\ 0 & \frac{\omega_{f}}{s+\omega_{f}}\end{array}\right] \tag{43}$$

where K_q is the droop coefficient of the reactive power loop, ω_f is the cut-off frequency of the low-pass filter.

The filter admittance $\mathbf{Y_L}$ is same to (28), and $\mathbf{Y_C}$ is

$$\mathbf{Y}_{\mathrm{C}}=\left[\begin{array}{cc}\frac{s}{(s^{2}+\omega^{2})C_{f}} & \frac{\omega}{(s^{2}+\omega^{2})C_{f}}\\ -\frac{\omega}{(s^{2}+\omega^{2})C_{f}} & \frac{s}{(s^{2}+\omega^{2})C_{f}}\end{array}\right]^{-1} \tag{44}$$

where C_f is the filter capacitance.

REFERENCES

[1] J. Sun, "Small-signal methods for ac distributed power systems–a review," *IEEE Transactions on Power Electronics*, vol. 24, no. 11, pp. 2545–2554, 2009.

[2] ——, "Impedance-based stability criterion for grid-connected inverters," *IEEE Transactions on Power Electronics*, vol. 26, no. 11, pp. 3075–3078, 2011.

[3] X. Wang and F. Blaabjerg, "Harmonic stability in power electronic-based power systems: Concept, modeling, and analysis," *IEEE Transactions on Smart Grid*, vol. 10, no. 3, pp. 2858–2870, 2019.

[4] B. He, W. Chen, H. Mu, D. Zhan, and C. Zhang, "Small-signal stability analysis and criterion of triple-stage cascaded dc system," *IEEE Journal of Emerging and Selected Topics in Power Electronics*, pp. 1–1, 2022.

[5] X. Wang, F. Blaabjerg, M. Liserre, Z. Chen, J. He, and Y. Li, "An active damper for stabilizing power-electronics-based ac systems," *IEEE Transactions on Power Electronics*, vol. 29, no. 7, pp. 3318–3329, 2014.

[6] Z.-X. Zou, G. Buticchi, and M. Liserre, "Analysis and stabilization of a smart transformer-fed grid," *IEEE Transactions on Industrial Electronics*, vol. 65, no. 2, pp. 1325–1335, 2018.

[7] B. He, W. Chen, X. Li, L. Shu, and X. Ruan, "A power adaptive impedance reshaping strategy for cascaded dc system with buck-type constant power load," *IEEE Transactions on Power Electronics*, pp. 1–1, 2022.

[8] L. Harnefors, M. Bongiorno, and S. Lundberg, "Input-admittance calculation and shaping for controlled voltage-source converters," *IEEE Transactions on Industrial Electronics*, vol. 54, no. 6, pp. 3323–3334, 2007.

[9] B. Wen, D. Boroyevich, R. Burgos, P. Mattavelli, and Z. Shen, "Analysis of d-q small-signal impedance of grid-tied inverters," *IEEE Transactions on Power Electronics*, vol. 31, no. 1, pp. 675–687, 2016.

[10] X. Wang, L. Harnefors, and F. Blaabjerg, "Unified impedance model of grid-connected voltage-source converters," *IEEE Transactions on Power Electronics*, vol. 33, no. 2, pp. 1775–1787, 2018.

[11] Z.-X. Zou and M. Liserre, "Modeling phase-locked loop-based synchronization in grid-interfaced converters," *IEEE Transactions on Energy Conversion*, vol. 35, no. 1, pp. 394–404, 2020.

[12] Z. Zou, B. D. Besheli, R. Rosso, M. Liserre, and X. Wang, "Interactions between two phase-locked loop synchronized grid converters," *IEEE Transactions on Industry Applications*, vol. 57, no. 4, pp. 3935–3947, 2021.

[13] J. L. Agorreta, M. Borrega, J. López, and L. Marroyo, "Modeling and control of n-paralleled grid-connected inverters with lcl filter coupled due to grid impedance in pv plants," *IEEE Transactions on Power Electronics*, vol. 26, no. 3, pp. 770–785, 2011.

[14] Z.-X. Zou, R. Rosso, and M. Liserre, "Modeling of the phase detector of a synchronous-reference-frame phase-locked loop based on second-order approximation," *IEEE Journal of Emerging and Selected Topics in Power Electronics*, vol. 8, no. 3, pp. 2534–2545, 2020.

[15] N. Pogaku, M. Prodanovic, and T. C. Green, "Modeling, analysis and testing of autonomous operation of an inverter-based microgrid," *IEEE Transactions on Power Electronics*, vol. 22, no. 2, pp. 613–625, 2007.

[16] S. Wang, Z. Liu, J. Liu, D. Boroyevich, and R. Burgos, "Small-signal modeling and stability prediction of parallel droop-controlled inverters based on terminal characteristics of individual inverters," *IEEE Transactions on Power Electronics*, vol. 35, no. 1, pp. 1045–1063, 2020.

[17] Y. Li, Y. Gu, Y. Zhu, A. Junyent-Ferré, X. Xiang, and T. C. Green, "Impedance circuit model of grid-forming inverter: Visualizing control algorithms as circuit elements," *IEEE Transactions on Power Electronics*, vol. 36, no. 3, pp. 3377–3395, 2021.

[18] J. Guo, Y. Chen, W. Wu, X. Wang, Z. Xie, L. Xie, and Z. Shuai, "Wide-band dq-frame impedance modeling of load-side virtual synchronous machine and its stability analysis in comparison with conventional pwm rectifier in weak grid," *IEEE Journal of Emerging and Selected Topics in Power Electronics*, vol. 9, no. 2, pp. 2440–2451, 2021.

[19] N. Bottrell, M. Prodanovic, and T. C. Green, "Dynamic stability of a microgrid with an active load," *IEEE Transactions on Power Electronics*, vol. 28, no. 11, pp. 5107–5119, 2013.

[20] R. Rosso, S. Engelken, and M. Liserre, "Robust stability investigation of the interactions among grid-forming and grid-following converters," *IEEE Journal of Emerging and Selected Topics in Power Electronics*, vol. 8, no. 2, pp. 991–1003, 2020.

[21] B. He, W. Chen, X. Ruan, X. Zhang, Z. Zou, and W. Cao, "A Generic Small-Signal Stability Criterion of DC Distribution Power System: Bus Node Impedance Criterion (BNIC)," *IEEE Transactions on Power Electronics*, vol. 37, no. 5, pp. 6116–6131, 2022.

[22] J. Dannehl, M. Liserre, and F. W. Fuchs, "Filter-based active damping of voltage source converters with lcl filter," *IEEE Transactions on Industrial Electronics*, vol. 58, no. 8, pp. 3623–3633, 2011.

[23] J. He, Y. W. Li, D. Bosnjak, and B. Harris, "Investigation and active damping of multiple resonances in a parallel-inverter-based microgrid," *IEEE Transactions on Power Electronics*, vol. 28, no. 1, pp. 234–246, 2013.

[24] M. Liserre, R. Teodorescu, and F. Blaabjerg, "Stability of photovoltaic and wind turbine grid-connected inverters for a large set of grid impedance values," *IEEE Transactions on Power Electronics*, vol. 21, no. 1, pp. 263–272, 2006.

[25] F. Blaabjerg, R. Teodorescu, M. Liserre, and A. V. Timbus, "Overview of control and grid synchronization for distributed power generation systems," *IEEE Transactions on Industrial Electronics*, vol. 53, no. 5, pp. 1398–1409, 2006.

[26] M. Liserre, G. Buticchi, M. Andresen, G. D. Carne, L. F. Costa, and Z. X. Zou, "The smart transformer: Impact on the electric grid and technology challenges," *IEEE Industrial Electronics Magazine*, vol. 10, no. 2, pp. 46–58, June 2016.

[27] L. Zhang, L. Harnefors, and H. Nee, "Power-synchronization control of grid-connected voltage-source converters," *IEEE Transactions on Power Systems*, vol. 25, no. 2, pp. 809–820, May 2010.

[28] Q. Zhong and G. Weiss, "Synchronverters: Inverters that mimic synchronous generators," *IEEE Transactions on Industrial Electronics*, vol. 58, no. 4, pp. 1259–1267, 2011.

[29] P. C. Loh, M. J. Newman, D. N. Zmood, and D. G. Holmes, "A comparative analysis of multiloop voltage regulation strategies for single and three-phase ups systems," *IEEE Transactions on Power Electronics*, vol. 18, no. 5, pp. 1176–1185, Sep. 2003.

[30] R. Rosso, X. Wang, M. Liserre, X. Lu, and S. Engelken, "Grid-forming converters: Control approaches, grid-synchronization, and future trends—a review," *IEEE Open Journal of Industry Applications*, vol. 2, pp. 93–109, 2021.

[31] J. M. Guerrero, J. C. Vasquez, J. Matas, M. Castilla, and L. Garcia de Vicuna, "Control strategy for flexible microgrid based on parallel line-interactive ups systems," *IEEE Transactions on Industrial Electronics*, vol. 56, no. 3, pp. 726–736, 2009.

[32] P. Rodriguez, C. Citro, J. I. Candela, J. Rocabert, and A. Luna, "Flexible grid connection and islanding of spc-based pv power converters," *IEEE Transactions on Industry Applications*, vol. 54, no. 3, pp. 2690–2702, 2018.

[33] S. D'Arco and J. A. Suul, "Equivalence of virtual synchronous machines and frequency-droops for converter-based microgrids," *IEEE Transactions on Smart Grid*, vol. 5, no. 1, pp. 394–395, 2014.

[34] C. Desoer and Y.-T. Wang, "On the generalized nyquist stability criterion," *IEEE Transactions on Automatic Control*, vol. 25, no. 2, pp. 187–196, 1980.

[35] L. Harnefors, "Modeling of three-phase dynamic systems using complex transfer functions and transfer matrices," *IEEE Transactions on Industrial Electronics*, vol. 54, no. 4, pp. 2239–2248, 2007.

[36] C. Wildrick, F. Lee, B. Cho, and B. Choi, "A method of defining the load impedance specification for a stable distributed power system," *IEEE Transactions on Power Electronics*, vol. 10, no. 3, pp. 280–285, 1995.

Zhixiang Zou (Senior Member, IEEE) received the B.Eng. and Ph.D. degrees in electrical and engineering from Southeast University, Nanjing, China, in 2007 and 2014, respectively, the Dr.-Ing. degree (summa cum laude) from Kiel University, Germany, in 2019. He was an engineer in the State Grid Electric Power Research Institute, Nanjing, China, from 2007 to 2009. He was a research fellow and lecturer at the Chair of Power Electronics, Kiel University, Germany, from 2014 to 2019. He is now an associate professor in the School of Electrical Engineering at the Southeast University. His research interests include smart transformers, microgrid stability, modeling and control of power converters.

Dr. Zou serves as Associate Editor for the IEEE Open Journal of Power Electronics and the IEEE Access, Secretary of IEEE Standard P3105, and Standing Director of IEEE PES Power System Relaying & Control Satellite Committee.

Jian Tang (Student Member, IEEE) was born in China, in 1999. He received the B.S. degree in electrical engineering in 2021 from Southeast University, Nanjing, China, where he is currently working toward the M.S. degree in electrical engineering. His research interests include the stability of power converters and the application of artificial intelligence on power converters.

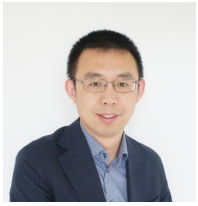

Xiongfei Wang (Senior Member, IEEE) received the B.S. degree from Yanshan University, Qinhuangdao, China, in 2006, the M.S. degree from Harbin Institute of Technology, Harbin, China, in 2008, both in electrical engineering, and the Ph.D. degree in energy technology from Aalborg University, Aalborg, Denmark, in 2013.

From 2009 he has been with the Department of Energy, Aalborg University (AAU Energy), where he became an Assistant Professor in 2014, an Associate Professor in 2016, a Professor and Leader of Electronic Power Grid (eGRID) Research Group in 2018. He has also been a part-time Professor at KTH Royal Institute of Technology, Stockholm, Sweden, from 2020. His current research interests include modeling and control of power electronic converters and systems, stability and power quality of power-electronics-dominated power systems, high-power converters.

Dr. Wang serves as Co-Editor-in-Chief for the IEEE TRANSACTIONS ON POWER ELECTRONICS and as Associate Editor for the IEEE JOURNAL OF EMERGING AND SELECTED TOPICS IN POWER ELECTRONICS (JESTPE). He has received 9 Prize Paper Awards in the IEEE Transactions and conferences, the 2016 AAU Talent for Future Research Leaders, the 2018 Richard M. Bass Outstanding Young Power Electronics Engineer Award, the 2019 IEEE PELS Sustainable Energy Systems Technical Achievement Award, the 2020 IEEE PES Prize Paper Award, the 2020 JESTPE Star Associate Editor Award, the 2022 Isao Takahashi Power Electronics Award, and the Highly Cited Researcher in the Web of Science from 2019.

Zheng Wang (Senior Member, IEEE) received the B.Eng. and the M.Eng. degrees from Southeast University, Nanjing, China, in 2000 and 2003, respectively, and the Ph.D. degree from the University of Hong Kong, Hong Kong, in 2008, all in electrical engineering.

From 2008 to 2009, he was a Postdoctoral Fellow in Ryerson University, Toronto, ON, Canada. He is currently a full Professor in the School of Electrical Engineering, Southeast University, China. His research interests include electric drives, power electronics, and distributed generation. In these fields, he has authored over 120 internationally refereed papers, 1 English book by IEEE-Wiley Press, and 2 English book chapters.

Prof. Wang received IEEE PES Chapter Outstanding Engineer Award, First-class Science and Technology Award of Jiangsu Province in China, and Outstanding Young Scholar Award of Jiangsu Natural Science Foundation of China. He is an IET Fellow and an associate editor of IEEE Transactions on Industrial Electronics.

Wu Chen (Senior Member, IEEE) was born in Jiangsu, China, in 1981. He received the B.S., M.S., and Ph.D. degrees in electrical engineering from the Nanjing University of Aeronautics and Astronautics (NUAA), Nanjing, China, in 2003, 2006, and 2009, respectively.

From 2009 to 2010, he was a Senior Research Assistant with the Department of Electronic Engineering, City University of Hong Kong, Hong Kong. In 2010 and 2011, he was a Postdoctoral Researcher with Future Electric Energy Delivery and Management Systems Center, North Carolina State University, Raleigh. Since September 2011, he has been an Associate Research Fellow with the School of Electrical Engineering, Southeast University, Nanjing, China, where he has been a Professor since 2016. His main research interests include soft-switching converters, power delivery, and power electronic system integration.

Dr. Chen is an Associate Editor for IEEE TRANSACTIONS ON INDUSTRIAL ELECTRONICS, JOURNAL OF POWER ELECTRONICS, and CPSS Transactions on Power Electronics and Applications.

Giampaolo Buticchi (Senior Member, IEEE) received the master's degree in electronic engineering and the Ph.D. degree in information technologies from the University of Parma, Italy, in 2009 and 2013, respectively. In 2012, he was a Visiting Researcher at the University of Nottingham, U.K. From 2014 to 2017, he was a Postdoctoral Researcher and a Guest Professor at the University of Kiel, Germany. In 2017, he was appointed as an Associate Professor in electrical engineering at the University of Nottingham Ningbo China and the Head of the Power Electronics of the Nottingham Electrification Center. He was promoted to a Professor, in 2020. He is author/coauthor of more than 230 scientific papers. His research interests include power electronics for renewable energy systems, smart transformer fed micro-grids, and dc grids for the more electric aircraft. He is one of the advocates for DC distribution systems and multi-port power electronics onboard the future aircraft.

Dr. Buticchi is the Chair of the IEEE-IES Technical Committee on Renewable Energy Systems and the IES Energy Cluster Delegate. During his stay in Germany, he was awarded with the Von Humboldt Postdoctoral Fellowship to carry out research related to fault tolerant topologies of smart transformers. He is an Associate Editor of the IEEE Transactions on Industrial Electronics, the IEEE Transactions on Transportation Electrification, and the IEEE Open Journal of the Industrial Electronics Society.

Marco Liserre (Fellow, IEEE) received the MSc and PhD degree in Electrical Engineering from the Bari Polytechnic, respectively in 1998 and 2002. He has been Associate Professor at Bari Polytechnic and from 2012 Professor in reliable power electronics at Aalborg University (Denmark). From 2013 he is Full Professor and he holds the Chair of Power Electronics at Kiel University (Germany). He has published 500 technical papers (1/3 of them in international peer-reviewed journals) and a book. These works have received more than 35000 citations. Marco Liserre is listed in ISI Thomson report "The world's most influential scientific minds" from 2014 and in Clarivate Analytics report "Highly Cited Researchers" from 2020.

He has been awarded with an ERC Consolidator Grant for the project "The Highly Efficient And Reliable smart Transformer (HEART), a new Heart for the Electric Distribution System".

He is member of IAS, PELS, PES and IES. He has been serving all these societies in different capacities. He has received the IES 2009 Early Career Award, the IES 2011 Anthony J. Hornfeck Service Award, the 2014 Dr. Bimal Bose Energy Systems Award, the 2011 Industrial Electronics Magazine best paper award and the Third Prize paper award by the Industrial Power Converter Committee at ECCE 2012, 2012, 2017 IEEE PELS Sustainable Energy Systems Technical Achievement Award and the 2018 IEEE-IES Mittelmann Achievement Award.